

Quasi-static magnetohydrodynamic turbulence at high Reynolds number

B. Favier^{1,3}, F.S. Godeferd^{1*}, C. Cambon¹, A. Delache², W.J.T. Bos¹

¹ LMFA UMR 5509 CNRS, École Centrale de Lyon, Université de Lyon, France.

² LMFA@UJM St-Étienne, CNRS UMR 5509

Université de St-Étienne, F-42023 Saint-Étienne Cedex 2, France.

³ School of Mathematics and Statistics, Newcastle University, UK.

Abstract

We analyse the anisotropy of homogeneous turbulence in an electrically conducting fluid submitted to a uniform magnetic field, for low magnetic Reynolds number, in the quasi-static approximation. We interpret disagreeing previous predictions between linearized theory and simulations: in the linear limit, the kinetic energy of transverse velocity components, normal to the magnetic field, decays faster than the kinetic energy of the axial component, along the magnetic field (Moffatt (1967)); whereas many numerical studies predict a final state characterised by dominant energy of transverse velocity components. We investigate the corresponding nonlinear phenomenon using Direct Numerical Simulations of freely-decaying turbulence, and a two-point statistical spectral closure based on the Eddy Damped Quasi-Normal Markovian model. The transition from the three-dimensional turbulent flow to a “two-and-a-half-dimensional” flow (Montgomery & Turner (1982)) is a result of the combined effects of short-time linear Joule dissipation and longer time nonlinear creation of polarisation anisotropy. It is this combination of linear and nonlinear effects which explains the disagreement between predictions from linearized theory and results from numerical simulations. The transition is characterized by the elongation of turbulent structures along the applied magnetic field, and by the strong anisotropy of directional two-point correlation spectra, in agreement with experimental evidence. Inertial equatorial transfers in both DNS and the model are presented to describe in detail the most important equilibrium dynamics. Spectral scalings are maintained in high Reynolds number turbulence attainable only with the EDQNM model, which also provides simplified modelling of the asymptotic state of quasi-static MHD turbulence.

Magnetohydrodynamics, Quasi-static hypothesis, Homogeneous turbulence, Direct Numerical Simulations, EDQNM

1 Introduction

In most geophysical and astrophysical flows, turbulence is affected by forces that distort significantly some of its scales in an anisotropic manner, such as the Coriolis force in rotating flows or the Lorentz force arising from the presence of an external magnetic field in a conducting fluid. This specific turbulent dynamics forced by an imposed magnetic field is found in liquid metal flows, be they of industrial, geophysical nature—the melted iron core of the earth—or of academic interest in the laboratory, such as the experiment by Alemany *et al.* (1979) in liquid mercury. Recent laboratory experiments on the dynamics of conducting fluids use sodium or gallium; liquid sodium is also used in industrial configurations, for instance in the French fast breeder reactor Superphénix.

Generally, the motion of turbulent liquid metals is governed by magnetohydrodynamics (MHD): the induction equation for the fluctuating magnetic field is added to the Navier-Stokes equations, which are in turn modified by the Lorentz force, representing the feedback from the magnetic

*Corresponding author: Fabien.Godeferd@ec-lyon.fr

field. In the presence of an external magnetic field, such MHD coupling results in new dissipative terms, of ohmic nature, and selectively damped waves, the Alfvén waves (Moffatt (1967)). In cases involving liquid metal, the magnetic diffusivity in the induction equation is larger than the molecular viscosity in the Navier-Stokes equations, *i.e.* the magnetic Prandtl number is small compared to one. The magnetic diffusivity is so large with respect to the kinematic diffusivity—with a magnetic Prandtl number less than 10^{-5} in the Earth’s iron core, of order 0.9×10^{-5} in liquid sodium or 1.4×10^{-7} in mercury—that it is consistent to consider the flow at very high Reynolds number and at low magnetic Reynolds number. In the following simulations, the magnetic Prandtl number is set to $Pr_M = 3.1 \times 10^{-4}$.

As discussed in section 2, if the magnetic Reynolds number is small enough, the linear regime no longer admits Alfvén waves solutions, and the effect of the Lorentz force reduces to an anisotropic ohmic (or Joule) dissipation term. In this regime, called the quasi-static approximation (QS MHD), the induction equation is simple enough to be solved explicitly and to yield a closed expression of the Lorentz force in terms of the velocity. The specificity of the quasi-static limit can be discussed both in terms of timescales and anisotropy. Unlike more general MHD turbulent flows, in which nonlinear and Alfvén timescales may be in competition and yield length scale dependent levels of anisotropy (see *e.g.* Zhou & Matthaeus (2005); Zhou (2010)), in QS MHD the magnetic diffusivity is too large to enable Alfvén waves. The only relevant timescales concern the modified Navier-Stokes equations, with a linear nondimensional timescale η/B_0^2 resulting from ohmic dissipation (B_0 is the external magnetic field, scaled as velocity, and η the magnetic diffusivity), and the nonlinear timescale l_0/u_0 (u_0 is the *rms* velocity and l_0 the length scale related to a turnover time). Strong anisotropy is first induced by the ohmic dissipation term over the linear timescale.

Quasi-static MHD turbulence was investigated experimentally by Alemany *et al.* (1979) and Caperan & Alemany (1985). In these studies, turbulence was generated by towing a grid through a cylindrical tank full of mercury, with an external magnetic field generated by a coil. Measurements include Reynolds stress components, an integral length scale in the axial direction and one-dimensional spectrum of transverse energy with respect to the axial wavenumber. A clear transition from a three-dimensional state, with conventional Kolmogorov spectrum, to a quasi-two-dimensional state, with k_{\parallel}^{-3} spectrum, was evidenced. The first phase of this 3D-2D transition was studied using axisymmetric Lin equations with an Eddy Damping Quasi-Normal Markovian (EDQNM) closure model by Cambon (1990), and the scenario of a two-dimensionalization in two steps was proposed. This scenario was recently confirmed by DNS in Favier *et al.* (2010) and one of the goals of the present paper is to go beyond the numerical approach of Cambon (1990) using both anisotropic EDQNM and direct numerical simulations (DNS). The “eddy-damping” rate appearing in the EDQNM closure for general MHD turbulence should in principle be modified to account for the combination of sweeping and straining mechanisms, thus allowing for the possibility of either Kolmogorov inertial scaling ($k^{-5/3}$ kinetic energy spectra, isotropized, *i.e.* spherically integrated) or Iroshnikov-Kraichnan scaling ($k^{-3/2}$) (see *e.g.* Zhou *et al.* (2004)). The QS MHD approximation, without Alfvénic propagation, allows to anchor the model within the classical hydrodynamic turbulence context, thus keeping the original damping consistent with Kolmogorov scaling.

Other numerical approaches in the same context are given by Schumann (1976), and Knaepen *et al.* (2004) with application to anisotropic modelling. A survey is offered by Knaepen & Moreau (2008), in which the change of anisotropic structure for the Reynolds stress tensor, from purely linear to nonlinear dynamics, is presented as an open problem. We think that this problem can be elucidated by the scenario of 3D-2D transition in two steps (Cambon (1990); Favier *et al.* (2010)) which is fully described hereafter.

Both spectral theory and DNS were applied by Ishida & Kaneda (2007) to the dynamical and structural study of the small scales anisotropy of QS MHD turbulence, while a recent approach by Okamoto *et al.* (2010) focused on the infrared limit, *i.e.* at very large scales. In the latter work, assuming the existence of a Loitsyanski-like invariant, decay laws for typical integral lengthscales and Reynolds stress components are proposed and compared to DNS results. The dynamics of integral length scales was shown to be crucial in rotating turbulence which bears strong analogies with MHD turbulence. For instance, the *linear* growth rate of the integral length scale related to transverse velocity components and axial separation, denoted ℓ_{\parallel} in Okamoto *et al.* (2010), and $L_{11}^{(3)} = L_{22}^{(3)}$ here, was clearly related to the role of *nonlinear* transfer terms (Cambon & Jacquin (1989); Jacquin *et al.* (1990); Cambon *et al.* (1997)). This result was recently recovered

by Staplehurst *et al.* (2008) with a different interpretation, although we believe that the use of axisymmetric Lin equations—equations for two-point velocity correlation spectra (von Kármán & Lin (1949))—, in which linear and nonlinear terms are exactly separated, is essential to the understanding. Accordingly, our theoretical approach is based on an anisotropic spectral formalism with generalized Lin equations instead of on a formalism based on the Kármán-Howarth equation, rather used by Okamoto *et al.* (2010), but bridges between the two approaches will be discussed in the following.

One of the most challenging aspects of quasi-static MHD turbulence, from a numerical point of view, is the rapid increase of the velocity correlation lengths in the direction of the imposed magnetic field. In that case, the results from classical pseudo-spectral methods with periodic boundary condition are often questionable, as the characteristic scale of the turbulent motion is no longer small compared to the numerical box size. In this paper, we compare Direct Numerical Simulations (DNS) with a model based on EDQNM closures and confirm that neither the low Reynolds numbers considered in DNS nor the confinement due to periodic boundary conditions alter our understanding of the dynamics. Secondly, our goal is to propose a detailed study of the anisotropy of quasi-static MHD turbulence at low, moderate and high Reynolds numbers. As in Favier *et al.* (2010), the analogy with the asymptotic quasi-two-dimensional state, called “two-and-a-half-dimensional” flow, will also be discussed.

The paper is organised as follows. The main parameters and governing equations are recalled in the following section. Spectral properties and EDQNM closures are discussed in section 3, and the numerical methods used in the paper are presented in section 4. Section 5 is devoted to the issue of confinement, both in DNS and EDQNM. Most of the results are gathered in section 6, where the statistical properties of quasi-static MHD turbulence are described, with an emphasis on anisotropy characterisation (section 6.2). Finally, the large Reynolds number behaviour is investigated in section 7.1, along with the analogy with quasi-two-dimensional turbulence in section 7.2. Details about EDQNM closed equations and linear predictions for the velocity correlation lengths are gathered in Appendices A and B.

2 Governing equations and parameters

We consider initially isotropic homogeneous turbulence in an incompressible conducting fluid, in which $u_x \simeq u_y \simeq u_z$, where u_x , u_y and u_z are the *rms* values of the velocity components. When the external magnetic field is applied, along z in the following, u_z will be called the *axial* component and u_x , u_y the *transverse* components. The fluid is characterised by the kinematic viscosity ν , density ρ and magnetic diffusivity $\eta = (\sigma\mu_0)^{-1}$; σ is the electrical conductivity, μ_0 the magnetic permeability. These physical properties are assumed to be constant. The integral length scale is l_0 , defined from the two-point velocity correlation tensor $R_{ii}(r) = \langle u_i(x_i)u_i(x_i+r) \rangle$, as $l_0 = \int_0^\infty R_{ii}(r)/R_{ii}(0)dr$, (or equivalently from the kinetic energy spectrum). The Reynolds number and its magnetic counterpart are $Re = (u_0l_0)/\nu \gg 1$ and $R_M = (u_0l_0)/\eta \ll 1$. The ratio between these two numbers defines the magnetic Prandtl number $Pr_M = \nu/\eta$, which is very small in our study. The flow is submitted to a uniform vertical magnetic field \mathbf{B} scaled as Alfvén speed as $\mathbf{B}_0 = \mathbf{B}/\sqrt{\rho\mu_0}$. The ratio between the eddy turnover time l_0/u_0 and the ohmic time η/B_0^2 is the magnetic interaction number $N = (B_0^2l_0)/(\eta u_0)$. Within the quasi-static approximation, which implies that R_M tends to zero, but which is nonetheless approximately valid for all $R_M < 1$ (Knaepen *et al.* (2004)), the Navier-Stokes equations become

$$\frac{\partial \mathbf{u}}{\partial t} + \mathbf{u} \cdot \nabla \mathbf{u} = -\frac{1}{\rho} \nabla p + \nu \nabla^2 \mathbf{u} + \underbrace{M_0^2 \Delta^{-1} \frac{\partial^2 \mathbf{u}}{\partial z^2}}_{\mathbf{F}} \quad (1)$$

where \mathbf{F} is the rotational part of the Lorentz force, Δ^{-1} is the inverse of the Laplacian operator, $M_0^2 = B_0^2/\eta$ and z the axial coordinate, along the direction of \mathbf{B}_0 . Compressible effects are not taken into account here, so that $\nabla \cdot \mathbf{u} = 0$.

3 Exact and model equations for two-point second-order statistics

We obtain hereafter the equations for the spectral statistics of the second-order moment of the fluctuating velocity field \mathbf{u} . The derivation is facilitated in two ways: first, by beginning with the Fourier coefficients of \mathbf{u} before computing the second-order moments; second, by using a Helmholtz-like decomposition in order to derive all the algebra only in terms of the incompressible components, namely the toroidal/poloidal decomposition.

Equation (1) for the velocity is 3D-Fourier transformed, with Fourier coefficients denoted with $\widehat{}$, and the pressure term is eliminated using incompressibility, introducing Kraichnan's projector

$$P_{imn}(\mathbf{k}) = -\frac{i}{2} \left[k_m \left(\delta_{in} - \frac{k_i k_n}{k^2} \right) + k_n \left(\delta_{im} - \frac{k_i k_m}{k^2} \right) \right], \quad (2)$$

so that

$$\left(\frac{\partial}{\partial t} + \nu k^2 + M_0^2 \cos^2 \theta \right) \hat{u}_i(\mathbf{k}, t) = P_{imn}(\mathbf{k}) \widehat{u_m u_n}, \quad (3)$$

where \mathbf{k} is the wave vector and θ its orientation with respect to the z -axis. The unique new term reflecting the quasi-static MHD effect is algebraic, $(M_0^2 \cos^2 \theta) \hat{u}_i(\mathbf{k}, t)$.

For second-order velocity correlations, the most general information is given by the second-order spectral tensor $\hat{R}_{ij}(\mathbf{k}, t)$ which in the homogeneous case is given by

$$\langle \hat{u}_j^*(\mathbf{p}, t) \hat{u}_i(\mathbf{k}, t) \rangle = \hat{R}_{ij}(\mathbf{k}, t) \delta^3(\mathbf{k} - \mathbf{p}). \quad (4)$$

The 3D Dirac function expresses that only the Fourier velocity components at the same wave vector have non zero double correlation. Another expression is obtained by considering a discretized velocity field, as in DNS (thus turning the mathematical formalism of distributions and generalized integrals, applied in continuous space, to classical integrals applied to discretized functions). For the particular case of a cubic periodic domain of size L , this replaces the Dirac term in the above equation by a factor $(L/(2\pi))^3$.

The brackets in equation (4) denote statistical ensemble averaging: in DNS started with a single realization of the velocity field, statistical averaging is obtained by spatial averaging, assuming ergodicity and using the particular symmetries preserved here, namely axisymmetry.

In the quasi-static MHD case under consideration, statistical symmetry is thus restricted to axisymmetry with mirror symmetry (the mean helicity is zero if initially zero), and the spectral tensor can be expressed in terms of toroidal and poloidal components of the velocity field in Fourier space. The two components are obtained using a polar-spherical frame of reference with base vectors $\mathbf{e}^{(1)}(\mathbf{k})$ and $\mathbf{e}^{(2)}(\mathbf{k})$ (*a.k.a.* Craya-Herring frame of reference, see figure 1; Herring (1974)), as

$$\hat{\mathbf{u}}(\mathbf{k}, t) = u^{(1)}(\mathbf{k}, t) \mathbf{e}^{(1)}(\mathbf{k}) + u^{(2)}(\mathbf{k}, t) \mathbf{e}^{(2)}(\mathbf{k}). \quad (5)$$

This decomposition automatically treats the velocity field as solenoidal, *i.e.* divergence free in physical space, through the algebraic orthogonality condition $\mathbf{k} \cdot \hat{\mathbf{u}}(\mathbf{k}) = 0$. In addition, it allows to construct any related statistical correlation, with a minimal number of components, for arbitrary anisotropy. The decomposition (5) is general, although, since it relies on the arbitrary choice of a polar axis, it is especially well suited to axisymmetric configurations, in which the tensors' dependence reduces to the wavenumber k and its angle θ to the axis.

The expression for the two-point second-order spectral tensor is therefore

$$\hat{R}_{ij} = \Phi^1 e_i^{(1)} e_j^{(1)} + \Phi^2 e_i^{(2)} e_j^{(2)}, \quad (6)$$

in which all the tensors and vectors depend on k and θ as the toroidal and poloidal energy tensors

$$\Phi^1(\mathbf{k}, t) = \Phi^1(k, \cos \theta, t), \quad \Phi^2(\mathbf{k}, t) = \Phi^2(k, \cos \theta, t). \quad (7)$$

Considering the symmetries of the flow, the most general decomposition in terms of energy density e , polarization \mathcal{Z} and helicity \mathcal{H} reduces to (Cambon & Jacquin (1989))

$$e(k, \cos \theta, t) = \frac{1}{2} (\Phi^1 + \Phi^2), \quad \mathcal{Z}(k, \cos \theta, t) = \frac{1}{2} (\Phi^2 - \Phi^1), \quad \mathcal{H}(\mathbf{k}, t) = 0. \quad (8)$$

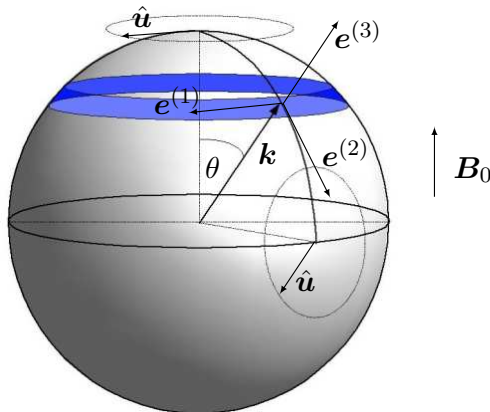


Figure 1: Craya-Herring frame ($\mathbf{e}^{(1)}, \mathbf{e}^{(2)}, \mathbf{e}^{(3)}$) in Fourier space. In the general case, Fourier modes in the blue region contribute to $E(k, \theta)$ (eq.(25)). However, if \mathbf{k} is vertical, the sum of the two components $u^{(1)}(\mathbf{k})$ and $u^{(2)}(\mathbf{k})$ generates a vertically sheared horizontal flow (VSHF), and if \mathbf{k} is horizontal, they correspond to transverse and axial components. Therefore, the polar modes ($\theta \simeq 0$) contribute to horizontal kinetic energy, whereas equatorial modes ($\theta \simeq \pi/2$) contribute to both axial (along $\mathbf{e}^{(2)}$) and transverse (along $\mathbf{e}^{(1)}$) kinetic energies.

The polarization term \mathcal{Z} is in general complex-valued and its imaginary part corresponds to a non zero cross-correlation between poloidal and toroidal velocity components. Here, \mathcal{Z} is real-valued and both sets of statistical quantities, Φ^1 and Φ^2 , or e and \mathcal{Z} are equivalent.

It is straightforward to derive the following exact equations for e and \mathcal{Z} :

$$\left(\frac{\partial}{\partial t} + 2\nu k^2 + 2M_0^2 \cos^2 \theta \right) e(k, \cos \theta, t) = T^{(e)}(k, \theta, t) \quad (9)$$

$$\left(\frac{\partial}{\partial t} + 2\nu k^2 + 2M_0^2 \cos^2 \theta \right) \mathcal{Z}(k, \cos \theta, t) = T^{(\mathcal{Z})}(k, \theta, t). \quad (10)$$

These equations are exact in the limit of homogeneous quasi-static MHD turbulence. They generalise the Lin equation, with the definition of cubic $T^{(e, \mathcal{Z})}$ terms given in Cambon & Jacquin (1989), and recalled in appendix A. All the terms in these equations can be obtained in pseudo-spectral DNS, as in Favier *et al.* (2010), using summation of Fourier modes on rings, in contrast with the summation of Fourier modes on spherical shells as usual in the analysis of isotropic turbulence (see figure 1). However, the anisotropic (k, θ) distribution of $T^{(e, \mathcal{Z})}$ is more affected by lack of sampling and noise in DNS, especially at small k where $\Delta k/k$ is large. It is therefore worthwhile to develop a model based on equations (9) and (10) to evaluate the behaviour of the second- and third-order moments—energy and energy transfer spectra. The model may then provide smooth values for these quantities, to be quantitatively compared to DNS results.

We will be using hereafter such a model, drawn from the anisotropic EDQNM closure theory, which has already been successfully applied to rotating or stably stratified turbulent flows, including a comparison with DNS (Cambon *et al.* (1997); Godefert & Staquet (2003)). In the derivation of the model, the toroidal/poloidal decomposition proves useful and valuable for simplifying the expressions for triple velocity correlations, without using projection operators inherited from equation (3). Another simplification comes from the use of a slightly modified decomposition of velocity, $\hat{\mathbf{u}}(\mathbf{k}, t) = \xi_+(\mathbf{k}, t)\mathbf{N}(\mathbf{k}) + \xi_-(\mathbf{k}, t)\mathbf{N}^*(\mathbf{k})$ analogous to (5), which brings out the helical modes ξ_{\pm} by projection onto $\mathbf{N}(\mathbf{k}) = \mathbf{e}^{(2)}(\mathbf{k}) - \mathbf{i}\mathbf{e}^{(1)}(\mathbf{k})$ and $\mathbf{N}^*(\mathbf{k}) = \mathbf{N}(-\mathbf{k})$. Helical modes are advantageous because they diagonalise the curl operator and allow a more compact decomposition of triple velocity correlations at three points (triadic terms), even in isotropic turbulence (see for example Waleffe (1992)). [In rotating turbulence, the helical modes are also the inertial waves modes, Cambon & Jacquin (1989); Waleffe (1993); Cambon *et al.* (1997); Bellet *et al.* (2006)]. The starting point of the closure is the third-order spectral tensor \mathbf{S} related to helical modes, defined by

$$\langle \xi_{s''}(\mathbf{q}, t) \xi_{s'}(\mathbf{p}, t) \xi_s(\mathbf{k}, t) \rangle = S_{ss's''}(\mathbf{k}, \mathbf{p}, t) \delta^3(\mathbf{k} + \mathbf{p} + \mathbf{q}). \quad (11)$$

The generalised Eddy Damping Quasi-Normal (EDQN) technique is then applied to the equation that governs the third-order spectral tensor,

$$\left[\frac{\partial}{\partial t} + \nu (k^2 + p^2 + q^2) + M_0^2 (\cos^2 \theta_k + \cos^2 \theta_p + \cos^2 \theta_q) \right] S_{ss's''}(\mathbf{k}, \mathbf{p}, t) = \Omega_{ss's''}(\mathbf{k}, \mathbf{p}, t), \quad (12)$$

in which $\Omega_{ss's''}(\mathbf{k}, \mathbf{p}, t)$ represents the contribution of fourth-order velocity correlations. In order to obtain a closed set of equations, Ω is expressed in terms of sums of products of double correlations. This would be an exact evaluation of the fourth-order moments, were it applied to a Gaussian random variable (the ‘QN’ part). We apply a corrective term (the ‘ED’ part) due to the non-vanishing fourth-order cumulant, to account for the departure from Gaussianity of both third-order and fourth-order cumulants. We shall use the version of the model that has provided the best results in rotating or stably stratified turbulence. This EDQNM2 model, say, accounts for the anisotropic Joule dissipation in both the second-order moments equation and in the third-order moments one (12). When informative, the results of EDQNM2 will also be contrasted with those of the simpler EDQNM1 model, which retains the Joule dissipation term only in the second-order moment equation, discarding it in equation (12). Contrasting both models allows to tell whether the main anisotropic mechanism is mostly linear or nonlinear. Additional information on the models is given in appendix A.

4 Numerical methods

To assess the validity of EDQNM closure in the context of quasi-static MHD turbulence and to obtain results at low and moderate Reynolds numbers, we perform Direct Numerical Simulations of equation (1) using a pseudo-spectral method implemented on a parallel computer. The velocity field is computed in a cubic box of side L with periodic boundary conditions using 512^3 Fourier modes. [The conventional shorthand relationship $L = 2\pi$ for non-dimensional DNS is used here, except for the previous discussion after equation (4).] A spherical 2/3-truncation of Fourier modes is used to avoid aliasing and the time scheme is third-order Adams-Bashforth. The dissipative viscous plus ohmic terms are treated implicitly.

The DNS results presented here are performed at higher resolution than those of Favier *et al.* (2010). An initially isotropic turbulent velocity field is created by a hydrodynamic simulation with large-scale forcing in order to reach a quasi-steady state. At the end of this pre-computation stage, the *rms* velocity is $u_0 = 0.81$ and the integral scale $l_0 = 0.25$ yielding $Re = u_0 l_0 / \nu \simeq 333$. The Reynolds number based on the Taylor microscale is $R_\lambda \simeq 95$. This rather low value, considering the resolution, is a consequence of our specific choice of a small initial integral scale l_0 , in order to lift partially the numerical confinement constraint, discussed in section 5. The corresponding turbulent flow field is used as initial state for two different MHD simulations. In all of them $R_M \simeq 0.1$ (hence $N \simeq 2$), so that the quasi-static approximation is justified (Knaepen *et al.* (2004)). Two different amplitudes of the imposed magnetic field are chosen, which correspond to two values of the interaction parameter: $N = 1$ and 5. For reference, we also compute the isotropic case, setting $B_0 = 0$, from the same initial condition. The quasi-static MHD simulations are freely decaying to avoid spurious effects of a forcing scheme on the development of anisotropy.

The two versions EDQNM1 and EDQNM2 mentioned above are used. The EDQNM simulations are initialised with the exact initial kinetic energy spectrum obtained from the DNS pre-computation. The EDQNM spectral space is discretized as follows: we use 64 values for the wave number k , 32 for the polar angle θ , and 32 internal orientations for the angle defining the orientation of the plane of the triads. In contrast to DNS, the wave number discretization used here is logarithmic, thereby improving the sampling of the large scales with respect to DNS. The minimum and maximum wave numbers solved are $k_{\min} = 1$ and $k_{\max} = 512/3$ as in DNS. If $B_0 = 0$, EDQNM1 and EDQNM2 are identical, and we also compute this particular case for comparison with isotropic DNS. Hereafter, DNS results are plotted with lines only, EDQNM results are plotted with lines and symbols (\circ for EDQNM1 results, \bullet for EDQNM2 results and \triangle for isotropic EDQNM).

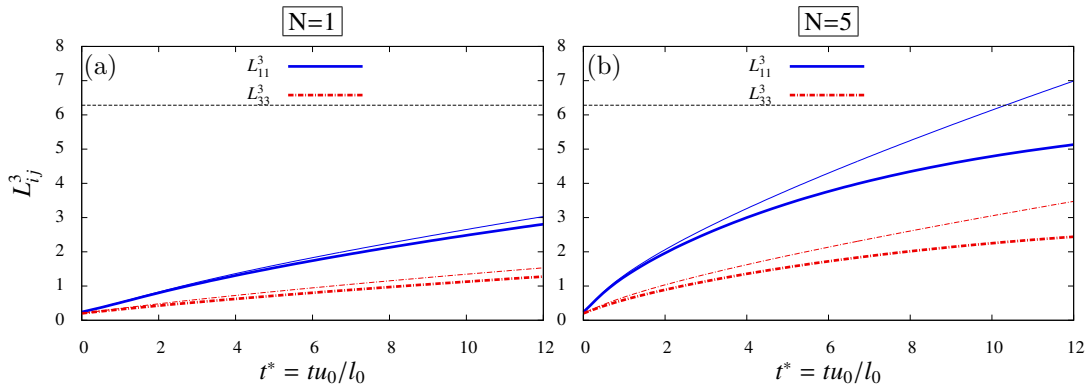


Figure 2: Velocity correlation lengths versus dimensionless time $t^* = tu_0/l_0$. The thick lines correspond to DNS without nonlinear interactions. The thin lines correspond to analytical linear predictions from Appendix B. The horizontal line presents the numerical limit of 2π .

5 Confinement due to periodic boundary conditions

This paragraph is specifically devoted to the problem of confinement in quasi-static MHD turbulence. As the anisotropic ohmic dissipation affects the flow, the velocity field rapidly homogenizes in the direction of the imposed magnetic field. The velocity correlation lengths thus increase in the axial direction. However, due to periodic boundary conditions used in DNS, these correlation lengths are limited by the size $L = 2\pi$ of the computational domain. To remove possible non physical effects due to this confinement, we compute the initial velocity field with an integral length scale about thirty times smaller than the numerical box size. We therefore adopt an intermediate configuration with moderate value of the Reynolds number.

It is not possible to evaluate the finite-size effects in the fully nonlinear case, especially because the theoretical study is based on additional assumptions. So we will restrict our analysis to the pure linear dynamics, or RDT. In so doing, we have to consider the following caveat: the pseudo-spectral method is assumed to be “exact” in the linear limit—to a given accuracy provided by the discretization in Fourier space—so that all RDT statistics derived from averaging $\hat{u}_i^* \hat{u}_j$ cannot be directly affected by the finite-size effect. On the other hand, statistics calculated from velocity components in physical space may be affected, even in the linear regime.

In order to assess the influence of the confinement and the validity of DNS in the context of quasi-static MHD turbulence, we perform two simulations, for $N = 1$ and 5 , in which the nonlinear advective term is neglected. (Several comparisons of this type between linear and nonlinear simulations can be found in Favier *et al.* (2010).) These simulations can be compared to the linear analytical solutions from Rapid Distortion Theory (see Moffatt (1967) and Appendix B). In order to study specifically the effect of confinement, we compute correlation lengths defined by

$$L_{ij}^{(l)} = \frac{1}{\langle u_i u_j \rangle} \int_0^\infty \langle u_i(\mathbf{x}) u_j(\mathbf{x} + \mathbf{r}) \rangle d\mathbf{r} \quad (13)$$

where $r_k = r \delta_{kl}$ is the two-point velocity separation. In the current axisymmetric flow, the most relevant anisotropy indicators are the integral length scales with axial separation, relative to either axial or transverse velocity components (Cambon & Jacquin (1989)):

$$L_{33}^{(3)} = \frac{2\pi^2}{\langle u_3^2 \rangle} \int_0^\infty [e(\mathbf{k}) + \Re \mathcal{Z}(\mathbf{k})] \Big|_{k_z=0} k dk \quad (14)$$

$$L_{11}^{(3)} = \frac{\pi^2}{\langle u_1^2 \rangle} \int_0^\infty [e(\mathbf{k}) - \Re \mathcal{Z}(\mathbf{k})] \Big|_{k_z=0} k dk . \quad (15)$$

The expressions of linear solutions for these quantities can be found in Appendix B. As discussed above, these quantities evaluated by DNS are expected to coincide with these analytical formulas only in the theoretical limit of a projection base with an infinite number of degrees of freedom.

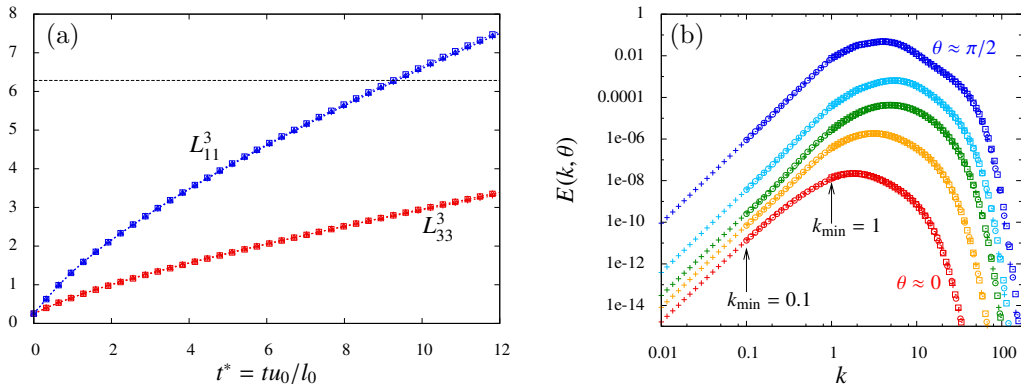


Figure 3: Results from EDQNM2 with different minimum wave number, from $k_{\min} = 0.01$ to $k_{\min} = 1$. (a) Velocity correlation lengths. The horizontal dotted line corresponds to the numerical limit of 2π , present in DNS. (b) Angular energy spectra at $t^* = 12$.

Figure 2 shows the correlation lengths $L_{33}^{(3)}$ and $L_{11}^{(3)}$ versus the dimensionless time $t^* = tu_0/l_0$, starting from the isotropic configuration at $t = 0$. The thick lines correspond to linearised DNS and thin lines correspond to linear analytical solutions. Both $N = 1$ and $N = 5$ cases are presented, for which one observes a growth of the correlation lengths, as expected in decaying turbulence. At moderate N , the length scales remain well below the numerical limit $L = 2\pi$, although one still notices a small departure between DNS and RDT results. The length scale predicted by analytical RDT is consistently larger than that of DNS. For $N = 5$, one clearly observes that the vertical correlation length $L_{11}^{(3)}$ saturates before the maximum value 2π whereas the linear solution continues to grow. This difference is a clear example of confinement in anisotropic DNS and cannot be attributed to nonlinearities, which are absent in these simulations.

Note that the initial integral length scale in the present DNS is very small ($l_0 \approx 0.25$) compared to the computational box size. Removing completely all trace of numerical confinement would require decreasing l_0 even more. Considering the current DNS resolution, the resulting Reynolds number would decrease too much for a turbulent flow to subsist. A solution is to increase the resolution, with increasingly demanding computational cost, to either a larger cubic box with resolution 2048^3 , or an adapted elongated box with resolution $512^2 \times 2048$, as done by Vorobev *et al.* (2005) in MHD turbulence, or in rotating turbulence by Cambon *et al.* (1997) and in convective turbulence by Matsumoto (2009). The latter option indeed delays the confinement issue, which is most pregnant in the axial direction, but also implies to some degree the anticipation of the anisotropy in the later stage of the evolution. In the following, we retain a 512^3 resolution consistent with the isotropy of initial conditions, considering only the early time response $t^* \leq 6$, hence keeping the flow in a significantly nonlinear regime while maintaining negligible confinement bias.

In order to investigate whether the mechanisms observed at these low Reynolds numbers will persist at higher Reynolds numbers, we will use EDQNM closures. It therefore makes sense to address also the problem of confinement in the numerical resolution of EDQNM. Such confinement limitations should in principle also apply to EDQNM models since the minimum wave number is, as in DNS, $k_{\min} = 1$. However, the closure model is written in spectral space so that periodic boundary conditions are not explicit. The EDQNM spectral resolution can easily be increased in order to quantify the impact of numerical confinement through the value of the minimum resolved wave number k_{\min} . We thus perform three EDQNM2 simulations (the results are the same using EDQNM1) in the case $N = 5$, with three different values $k_{\min} = 0.01, 0.1, 1$. Firstly, the time evolution of the velocity correlation lengths $L_{33}^{(3)}$ and $L_{11}^{(3)}$ are plotted in figure 3(a). The predictions from the three simulations are almost undistinguishable, and, in contrast with the DNS results of figure 2(b), the growth of correlation lengths is not constrained by the value of the minimum wave number. Secondly, angular energy spectra, plotted on figure 3(b) at $t^* = 12$, show that the spectral anisotropy is the same whatever k_{\min} (details on the anisotropic spectra will be presented in section 6.2). Accordingly, we choose $k_{\min} = 1$ in the following, to allow a complete comparison with DNS results, with the understanding that EDQNM is free from truncation effects.

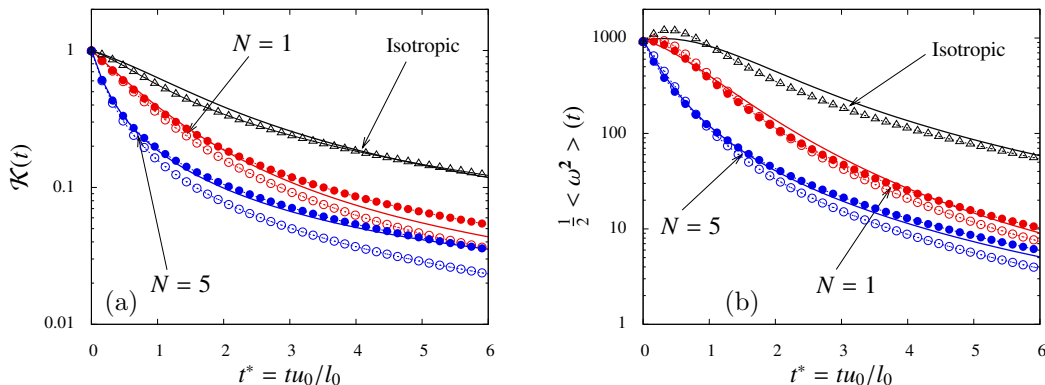


Figure 4: Kinetic energy $\mathcal{K}(t)$ and enstrophy $\langle \omega^2 \rangle / 2$ versus dimensionless time t^* in log-linear scale. — DNS, \circ EDQNM1, \bullet EDQNM2, \triangle isotropic EDQNM.

6 Comparison between DNS and EDQNM

In this section, we propose a comparison between DNS and EDQNM results at moderate Reynolds number. In the context of quasi-static MHD turbulence, it is hardly possible with DNS to reach high Reynolds number simulations without encountering artificial effects of the periodic boundary conditions, in view of the rapidly increasing numerical cost of pseudo-spectral methods with Re . In this section, we shall compare statistics obtained from the flow field predicted by DNS with data directly derived from EDQNM models, for a Reynolds number attainable by DNS. We first present a comparison of dynamical quantities in section 6.1, then an extended analysis of anisotropy in section section 6.2.

6.1 Energetics

Total kinetic energy and total enstrophy are presented in figures 4(a) and (b) respectively. After initialisation, the EDQNM model instantaneously builds triple correlations, or, in other terms, energy transfer spectra, close to the ones observed in DNS. Therefore, the initial dynamics for the EDQNM1-2 models and DNS are similar. At larger times $t^* > 1$, and for $N = 1$, EDQNM2 (*resp.* EDQNM1) seems to overestimate (*resp.* underestimate) the value of kinetic energy. For $N = 5$, the kinetic energy and enstrophy decays predicted by EDQNM2 and DNS are in good agreement. In both cases, it appears that EDQNM1 underestimates the kinetic energy and the enstrophy after the initial short time stage, whereas EDQNM2 predicts decay rates that are remarkably close to the DNS evolution, if one considers all the possible sources of statistical inaccuracies which may appear in DNS data. The good performance of EDQNM2 with respect to EDQNM1 is clearly the sign that including the explicit effect of anisotropic Joule dissipation in the nonlinear dynamics is crucial for modelling quasi-static MHD turbulence. The scale-dependent Joule dissipation timescale $\tau_M(k) = 1/M_0$ can thus be compared to the turbulent timescale $\tau(k) = \varepsilon^{-1/3} k^{-2/3}$, where ε is the kinetic energy dissipation. Equating these timescales yields a given wavenumber $k_M = M_0^3 \varepsilon^{-1/2}$, say, which separates Joule dissipation dominated scales $k < k_M$ from dominant nonlinear dynamics $k > k_M$ ($1/k_M$ is the equivalent of the Ozmidov scale introduced in stably stratified turbulence). For our runs at $N = 1$, $k_M = 5$ initially, and $k_M = 50$ at the end of the simulation, whereas for the run $N = 5$, the figures are 60 at the beginning, and 800 in the end. This shows that, apart from the early stage of the $N = 1$ case, in all our simulations, the energetic scales are dominated by ohmic dissipation (this is illustrated on figure 10).

The axisymmetric EDQNM model is also valid for isotropic turbulence, but the numerical cost is considerably larger than that of the classical fully isotropic model. The results of isotropic DNS (*i.e.* setting $B_0 = 0$), presented on figure 4, are obtained from the same initial conditions, and show that the decay of kinetic energy is faster in the QS MHD case than in isotropic turbulence due to the additional ohmic dissipation. Concerning the evolution of enstrophy, one observes an initial increase for both EDQNM models in the isotropic case and in DNS, showing a short-time

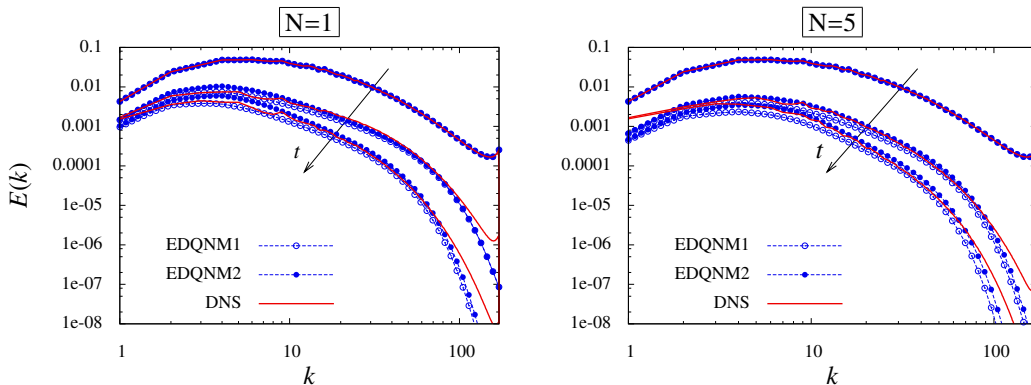


Figure 5: Kinetic energy spectra at dimensionless times $t^* = 0, 3$ and 6 .

re-adjustment which cannot occur when the interaction parameter N is large, since the magnetic effect catches up almost instantaneously.

The kinetic energy spectra are plotted in figure 5 at three different times. The initial energy spectra are identical, since EDQNM spectra are initialized from DNS results. As already mentioned the initial integral length scale (*resp.* peak energy wave number) is smaller (*resp.* larger) than for classical hydrodynamic simulations. Figure 5 shows that the DNS and EDQNM2 spectral energy levels are in good agreement for all the scales of the flow. For $N = 1$ (figure 5a), the slight overestimation of the energy by EDQNM2 is again observed, particularly at intermediate scales $6 < k < 12$, while we retrieve the larger underprediction of the EDQNM1 model. In all cases, the comparison between DNS and EDQNM in the dissipative range of the spectrum is not as good independently of the value of N and of the model version. Several explanations can be put forward, both on the account of the model or of the DNS approach: desaliasing in DNS, intermittency not present in the EDQNM model, truncation in both, *etc.* Overall, figure 5 still demonstrates that the EDQNM2 model is a good predictive model of the dynamics of QS MHD over a wide range of scales.

6.2 Refined comparison of the anisotropy

The level of anisotropy in the flow can be quantified with increasing refinement degrees. A first measure is the ratio between horizontal and vertical kinetic energies, plotted in figure 6(a). The linear and inviscid regimes are characterised by the following scaling (Moffatt (1967))

$$\langle u_{\parallel}^2 \rangle \simeq 2 \langle u_{\perp}^2 \rangle, \quad (16)$$

where $u_{\parallel} = u_z$ is the axial velocity component, and $u_{\perp} = \sqrt{u_x^2 + u_y^2}$, with u_x and u_y the transverse velocity components. As already observed by Vorobev *et al.* (2005), Burattini *et al.* (2008a), Favier *et al.* (2010), this linear prediction is not observed in numerical simulations. The initial stage ($t^* < 1$) is characterised by a decrease of the ratio $r_e = \langle u_{\perp}^2 \rangle / \langle u_{\parallel}^2 \rangle$, in agreement with equation (16), but after a few turnover times, this ratio increases. It was shown that this is not due to a restoration of isotropy but to a nonlinear phenomenon linked to the particular quasi-two-dimensional structure of the flow (for details, see Favier *et al.* (2010) and section 7.2). Figure 6(a) shows that EDQNM2 reproduces this departure from the linear prediction, although with a time lag and a smaller amplitude. At small interaction parameter, EDQNM2 provides a better agreement with DNS than EDQNM1 for $N = 1$, less so for $N = 5$.

The ratio between transverse and axial kinetic energies presented on figure 6(a) sets the focus on the large scale dynamics. The small scale dynamics can be brought forward by computing a similar quantity based on vorticity components. We define the ratio between transverse and axial enstrophies as

$$r_{\omega} = \frac{\langle \omega_{\perp}^2 \rangle}{\langle \omega_{\parallel}^2 \rangle}. \quad (17)$$

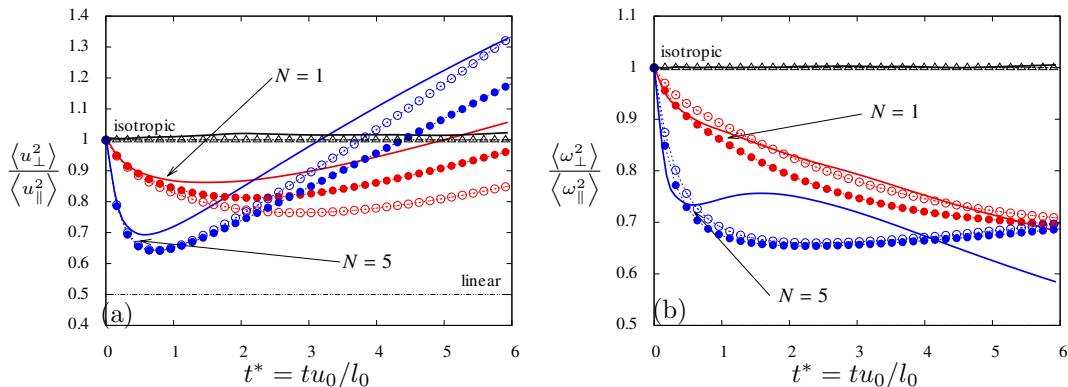


Figure 6: (a) Ratio between horizontal and vertical kinetic energies versus dimensionless time $t^* = tu_0/l_0$. (b) Ratio between horizontal and vertical enstrophies versus dimensionless time $t^* = tu_0/l_0$. — DNS, \circ EDQNM1, \bullet EDQNM2, \triangle Isotropic EDQNM.

In a pure two-dimensional case, this ratio goes to zero, whereas in the isotropic case, it is about one. For $N = 1$ on figure 6(b), the ratio is always decreasing independently of the model considered, but is far from the two-dimensional value. For $N = 5$, there is a clear departure between DNS and EDQNM predictions. Initially in DNS, there is a strong decay of r_ω , then the trend is reversed synchronously with the decay reversal of r_e (figure 6a), at $t^* \approx 1$. Eventually, r_ω decreases again. This three-stage evolution is not captured by the EDQNM model. The first increase stage after the initial decrease is reproduced, with a delay as for r_e , but the second change of slope is not. It seems that a phenomenon appears in DNS at $t^* \approx 2-3$, whereby the ratio r_ω decreases in DNS, which is not captured by the model. The multiplicity of possible nonlinear time scales in MHD turbulence might not be reproduced by the single time scale introduced in the closure (equation 33).

Let us now compare the DNS and EDQNM results concerning the prediction of the directional anisotropy resulting from ohmic dissipation. The first effect of the magnetic field is to dissipate preferentially Fourier modes with wave vector \mathbf{k} parallel to \mathbf{B}_0 . A direct consequence is the decrease of the transverse kinetic energy with respect to the axial one (since modes with $\mathbf{k} \parallel \mathbf{B}_0$ contribute only to transverse energy, see figure 1). This is observed in figure 6(a).

The simplest way to quantify this directional anisotropy (*directivity*) is to consider typical angles defined in physical space, such as the ones introduced by Moreau and Shebalin (Alemany *et al.* (1979); Shebalin *et al.* (1983)). The ‘Moreau angle’ β defined by

$$\cos^2 \beta(t) = (\mathcal{K}(t))^{-1} \iiint \cos^2 \theta e(\mathbf{k}, t) d^3 \mathbf{k}, \quad (18)$$

directly derives from the one-point dynamical equation for the kinetic energy $\mathcal{K}(t) = \iiint e(\mathbf{k}, t) d^3 \mathbf{k}$

$$d\mathcal{K}/dt + 2M_0^2 \cos^2 \beta \mathcal{K} = -\varepsilon \quad (19)$$

coming from integration of equation (9). This equation suggests as well to refine the definition of the separating wavenumber introduced in section 6.1 as $k_M = M_0^3 \cos^3 \beta \varepsilon^{-1/2}$.

The Shebalin angle, more widely used in the MHD community, characterizes the angular distribution of the vorticity spectrum $k^2 e$, as evidenced by its definition contrasted with equation (18):

$$\cos^2 \theta_u(t) = (\langle \omega^2 \rangle(t))^{-1} \iiint k^2 \cos^2 \theta e(\mathbf{k}, t) d^3 \mathbf{k}, \quad (20)$$

where the enstrophy is $\langle \omega^2 \rangle = \iiint k^2 e(\mathbf{k}, t) d^3 \mathbf{k}$. This definition is the continuous counterpart, in a slightly different form, of the classical discretized version Shebalin *et al.* (1983), used for the plots in figure 7(a):

$$\tan^2 \theta_u = \frac{\sum_{\mathbf{k}} k_{\perp}^2 |\hat{\mathbf{u}}(\mathbf{k}, t)|^2}{\sum_{\mathbf{k}} k_{\parallel}^2 |\hat{\mathbf{u}}(\mathbf{k}, t)|^2}, \quad (21)$$

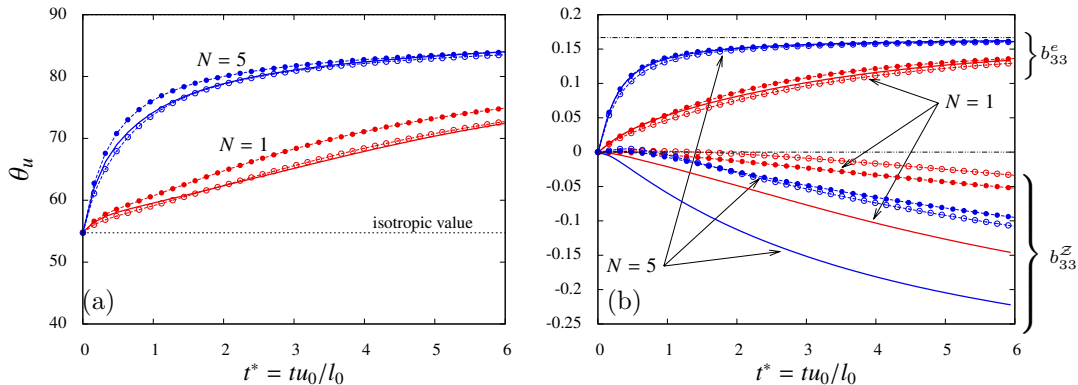


Figure 7: Anisotropic coefficients versus dimensionless time $t^* = tu_0/l_0$. (a) Shebalin angle θ_u . (b) Anisotropic part of the Reynolds stress tensor $b_{33} = b_{33}^e + b_{33}^Z$. — DNS, \circ EDQNM1 and \bullet EDQNM2.

where $k_\perp = \sqrt{k_x^2 + k_y^2}$ is the transverse component of the wave vector, and $k_\parallel = k_z = k^2 \cos^2 \theta$ is the axial one. On the other hand, we do not plot directly the Moreau angle here, but the equivalent quantity b_{33}^e defined by equation (22): b_{33}^e is proportional to the intensity of the first angular harmonic of e , through $b_{33}^e = 1/6 - (1/2) \cos^2 \theta$.

The Shebalin angles for the velocity field are first plotted in figure 7(a). In all cases —and similarly for the Moreau angles—, the increase from the isotropic initial value $\theta_u \approx 54.7^\circ$ indicates a concentration of energy in modes perpendicular to the imposed magnetic field. This two-dimensional limit corresponds to $\theta_u \approx 90^\circ$. This is a well-known consequence of the ohmic dissipation, which results in physical space in a flow invariant in the axial direction. We note that EDQNM2 overpredicts the value of the Shebalin angle with respect to EDQNM1 and DNS. This overestimation does not concern b_{33}^e , as shown in figure 7(b). This suggests that the EDQNM prediction for the directional anisotropy is different for larger scales (energy distribution) and smaller scales (vorticity distribution), with a particular sensitivity of EDQNM2 at smaller scales. A small inaccuracy can therefore pull the Shebalin angle predicted by EDQNM2 in the wrong way, even if EDQNM2 gives a better overall prediction than EDQNM1.

The *polarization* anisotropy is another kind of anisotropy that may appear in addition to the directional anisotropy. This anisotropy cannot be quantified with Shebalin angles, since it is not directly related to the dependence of the poloidal and toroidal velocity components upon θ , but is related to their difference. Its characterization requires a specific splitting of the deviatoric part $b_{ij} = R_{ij}/(2\mathcal{K}) - \delta_{ij}/3$ of the Reynolds tensor $R_{ij} = \langle u_i(\mathbf{x})u_j(\mathbf{x}) \rangle$, where \mathcal{K} is the total kinetic and δ_{ij} the Kronecker tensor. Considering the axisymmetry of the flow about the axis of \mathbf{B}_0 , only one diagonal term is needed to describe the anisotropy, b_{33} say. Using equations (6) and (8), one obtains the two contributions for $b_{33} = b_{33}^e + b_{33}^Z$ (Cambon & Jacquin (1989); Cambon *et al.* (1997)), with:

$$b_{33}^e = \frac{1}{2\mathcal{K}} \int \left(e(\mathbf{k}) - \frac{E(k)}{4\pi k^2} \right) \sin^2 \theta d^3 \mathbf{k} \quad (22)$$

$$b_{33}^Z = \frac{1}{2\mathcal{K}} \int \mathcal{Z}(k) \sin^2 \theta d^3 \mathbf{k} \quad (23)$$

where θ is the polar angle between the wave vector \mathbf{k} and the axis of symmetry (see figure 1), $E(k)$ is the spherically-averaged kinetic energy spectrum, $\mathcal{Z}(k)$ is the polarization spectrum. As stated by its definition (22), b_{33}^e is similar to the Shebalin angles in that it quantifies the directivity of the energy with respect to the vertical direction. b_{33}^Z quantifies the additional dimensionality anisotropy which is conveyed by the polarization spectrum \mathcal{Z} . The limiting value $b_{33}^e = 1/6$ is reached for two-dimensional flows, in both the 2D-3C and the 2D-2C cases, distinguished only by the value of b^Z : 0 for 2D-3C flows, $-1/2$ for 2D-2C flows.

Figure 7(b) presents the evolution of b_{33}^e and b_{33}^Z versus time. Concerning b_{33}^e , the same conclusions as the ones resulting from the Shebalin angles are drawn from the figure. Note that it

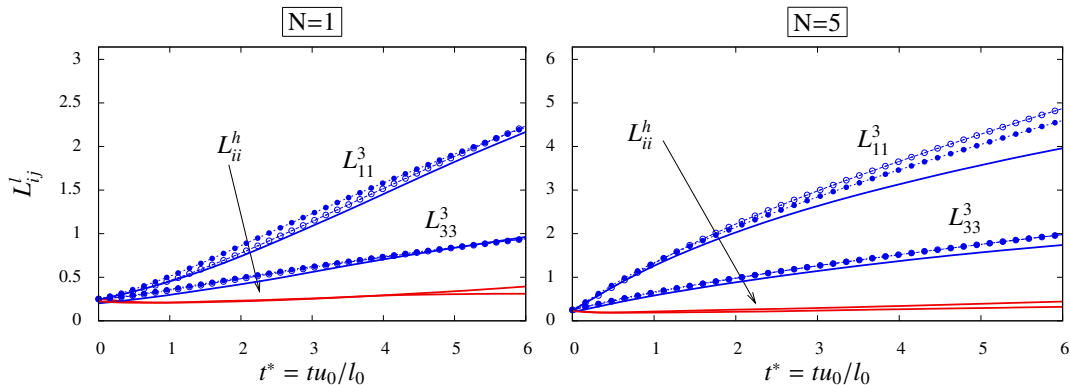


Figure 8: Velocity correlation lengths for $N = 1$ (left) and $N = 5$ (right). Superscripts 3, h and i correspond to vertical direction (aligned with \mathbf{B}_0), horizontal direction and any direction, respectively. — DNS, \circ EDQNM1 and \bullet EDQNM2.

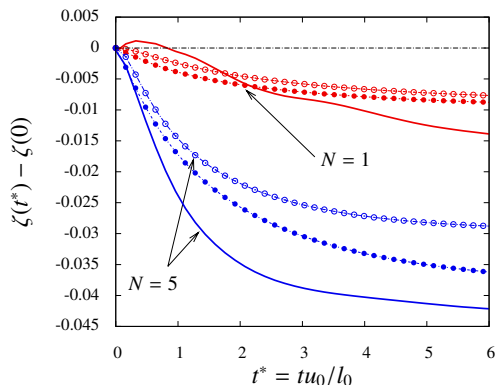


Figure 9: Evolution with time of $\zeta = \langle u_3^2 \rangle L_{33}^{(3)} - 2\langle u_1^2 \rangle L_{11}^{(3)}$. — DNS, \circ EDQNM1 and \bullet EDQNM2.

is possible to rescale time with the ohmic dissipation characteristic time so that both b_{33}^e and θ_u collapse independently of the intensity of B_0 (Favier *et al.* (2010) and analytical law in appendix B).

The polarization part b_{33}^z , which is zero initially, decays in all cases, showing a global predominance of toroidal over poloidal energy. Negative polarization is thus responsible for the increase of the componental enstrophy and velocity ratios r_ω and r_e plotted in figure 6. EDQNM1-2 models underestimate the amplitude of polarization, but this is not necessarily a defect of the closure, given the spurious confinement effects yielding polarization in DNS, as shown and discussed in section 5. As already observed, EDQNM2 is in better agreement with DNS for $N = 1$ (when nonlinearities are important) whereas EDQNM1 compares better for $N = 5$ (when nonlinearities are dominated by ohmic dissipation). In view of the value of the separation scale k_M presented in section 6.1, the dynamics is driven by nonlinear timescale only at the beginning of the simulation at $N = 1$. As mentioned in the Introduction, the additional physics injected into the EDQNM2 model through the straining timescale (see Appendix A) is corrected by the Joule dissipation time-scale, but the imbalance of the two acts variably depending on the regime. It seems here that the EDQNM2 nonlinear improvements are too large for these Joule dissipation dominated scales.

We then consider the time evolution of the velocity correlation lengths defined by equations (13), presented on figure 8. At the end of the simulations ($t^* \approx 6$), $L_{33}^{(3)} \approx 2.2$ and 0.98 for the respective cases $N = 5$ and 1 . The axial correlation length of axial velocity $L_{33}^{(3)}$ is therefore always significantly smaller than the box size 2π . The axial correlation length of transverse velocity, however, for the case at $N = 5$, reaches about two thirds of the numerical box size. The correlation lengths obtained from EDQNM are close to the ones computed from DNS results, indicating a good prediction of the anisotropy of the large scale structures of the flow. As previously discussed in section 5, the growth of $L_{11}^{(3)}$ computed by DNS seems to slow down in time, a fact that can be attributed to

the periodic boundary conditions. Such saturation is not apparent in EDQNM results, so that the correlation lengths continue to grow. The confinement-related explanation is supported by the similitude between figure 2(b) and 8(b).

Moreover, it is possible to isolate the contribution due to polarization by computing

$$\zeta = \langle u_3^2 \rangle L_{33}^{(3)} - 2\langle u_1^2 \rangle L_{11}^{(3)} = \int_0^\infty 4\pi^2 \Re \mathcal{Z}(\mathbf{k}) \Big|_{k_z=0} k dk . \quad (24)$$

This quantity is interesting for two reasons: (a) from equations (14) and (15), its departure from zero is only due to the polarization $\mathcal{Z}(\mathbf{k})$; (b) this quantity is accessible experimentally. Initially, ζ is exactly zero for EDQNM models since the polarization is set to zero at the beginning of the calculation. However, $\zeta(t^* = 0) = -0.015$ in DNS is small but not exactly zero. This may be a trace of the forcing scheme used to reach a quasi-steady state of hydrodynamic turbulence for $t^* < 0$. ζ may also be dominated by contributions from small values of k_z , where the DNS spectral discretization is too coarse to yield converged statistics. In all cases, figure 9 shows that $\zeta(t^*) - \zeta(0)$ decreases, in accordance with negative polarization. One observes that the equatorial polarization is underpredicted by EDQNM, which is consistent with the previous observations on the deviatoric tensor b_{33} . However, the relative evolutions of the $N = 1$ and $N = 5$ EDQNM predictions for ζ agree correctly with the dependence with N observed on the DNS curves.

All the previous statistics involve a spectral integration over wave numbers, so that information about scale dependency is lost. On the contrary, the angular spectrum $E(k, \theta)$ retains both scale- and angle-dependence:

$$E(k, \theta) = \left[\int_{\theta-\Delta\theta/2}^{\theta+\Delta\theta/2} \cos \theta d\theta \right]^{-1} \sum_{\substack{k-\Delta k/2 < |\mathbf{k}| < k+\Delta k/2 \\ \theta-\Delta\theta/2 < \theta < \theta+\Delta\theta/2}} \hat{u}_i(k, \theta) \hat{u}_i^*(k, \theta) . \quad (25)$$

where Δk and $\Delta\theta$ specify the discretization steps in Fourier space used for computing the anisotropic spectra (see figure 1 in which the shaded region corresponds to the scales which contribute to $E(k, \theta)$). Ring-averaged angular spectra $E(k, \theta)$ have already been used in the context of rotating turbulence by Cambon *et al.* (1997) and for stably stratified turbulence by Godeferd & Staquet (2003), and are similar to the ring decomposition by Burattini *et al.* (2008b). We choose here $\Delta k = 1$ and $\Delta\theta = \pi/10$, figures that depend on the DNS resolution to ensure optimal statistical sampling. The angular spectra are plotted on figure 10, at time $t^* = 5$. At the initial time $t^* = 0$, all angular spectra collapse since the initial condition is isotropic. Figure 10 shows that, as time increases, most of the kinetic energy is concentrated in the spectrum with transverse wavevectors, since the Joule dissipation term in equation (9) reduces less energy at this orientation, independently on the wavenumber. The qualitative agreement of EDQNM model predictions with the DNS ones is impressive, considering the multi-scale, multi-directional character of these spectral statistics. There are, however, some differences. First, one observes that EDQNM2 overestimates slightly the equatorial kinetic energy, which is consistent with the overestimation of the Shebalin angle already observed in figure 7(a). However, the global angular dependency of the energy observed in DNS is well reproduced by EDQNM2, whereas EDQNM1 overestimates the polar kinetic energy (see lowermost curves with \circ symbols on figure 10). In all models, as N increases, the angular anisotropy increases so that the flow tends to be invariant in the vertical direction.

So far, we focused on the angular dependency of the kinetic energy. The departure from isotropically distributed energy is due to Joule dissipation and is observable in the growth of the Shebalin angle θ_u (see figure 7(a)), b_{33}^e (see figure 7(b)), and in angular spectra. However, it has been demonstrated that this effect is mostly linear, and that it can explain neither negative values of b_{33}^z (see figure 7(b)), nor the increase of the ratio between transverse and axial energies at large times (see figure 6). The poloidal/toroidal decomposition of spectral quantities (equation (6)), along with the angular spectral distribution, provides a way of understanding these unexplained features. Figure 11 presents the equatorial spectra (*i.e.* only transverse wave vectors are considered) decomposed as poloidal (*i.e.* axial in this particular case, see figure 1) and toroidal (*i.e.* transverse in this configuration) contributions. The *polarization* anisotropy is clearly observable, as the difference between the two spectra. It is scale-dependent, with negative polarization at large scales ($\Phi^1 > \Phi^2$), responsible for the negative value of b_{33}^z and positive polarization at small scales

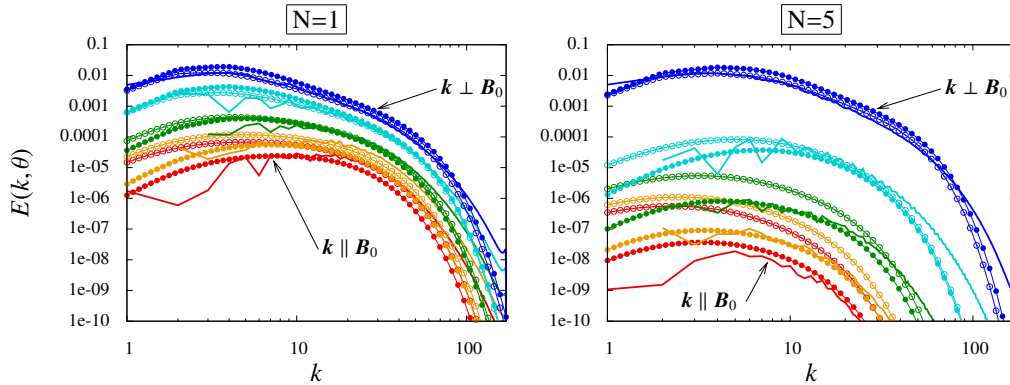


Figure 10: Angular energy spectra at $t^* = 5$. — DNS, \circ EDQNM1 and \bullet EDQNM2. In each case, five curves are plotted, from top/equator ($\mathbf{k} \perp \mathbf{B}_0$) to bottom/pole ($\mathbf{k} \parallel \mathbf{B}_0$). $N = 1$ (left) and $N = 5$ (right).

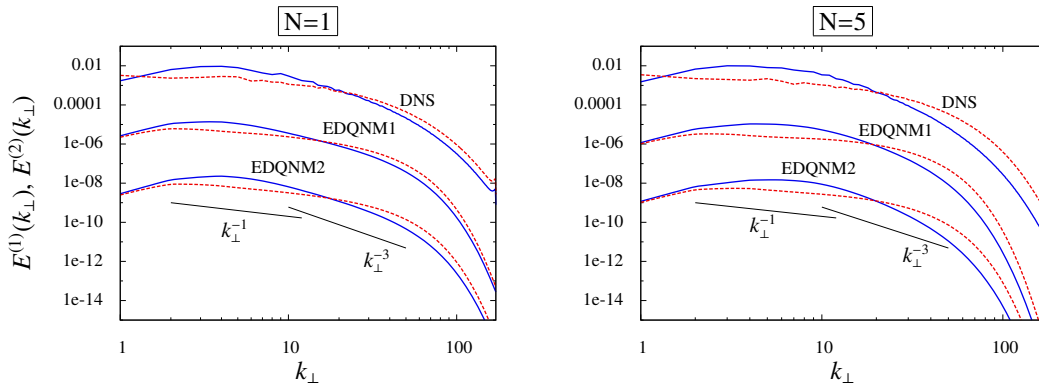


Figure 11: Equatorial energy spectra at $t^* = 6$. The solid blue lines correspond to $\Phi^{(1)}(k_{\perp})$, the dotted red lines correspond to $\Phi^{(2)}(k_{\perp})$. EDQNM1 results are shifted down by three decades, EDQNM2 ones are shifted down by six decades.

($\Phi^1 < \Phi^2$). The structure of the flow is therefore strongly scale-dependent with dominance of transverse kinetic energy at large scales and a dominance of axial kinetic energy at small scales. This departure from the poloidal/toroidal equipartition of energy is mainly observable for transverse wavevectors, where the energy accumulates because of ohmic dissipation. For axial wavevectors, θ goes to zero and this is no longer observable. Note that the cross-over wave number k_{\perp}^c at which $\Phi^1(k_{\perp}^c) = \Phi^2(k_{\perp}^c)$ ($k_{\perp}^c \approx 20$ on figure 11) depends mainly on the initial conditions and on the Reynolds number. Both EDQNM1-2 models reproduce this non-linear behaviour as well as the approximate location of the cross-over wave number.

k_{\perp}^{-3} and k_{\perp}^{-1} slopes are indicated on figure 11 for comparison with common scalings of two-dimensional turbulence with passive scalar (see Batchelor (1959), Bos *et al.* (2009), and the discussion of the analogy with two-dimensional three components flows in section 7.2).

6.3 Dynamical equilibrium and energy transfer spectra

The anisotropic re-distribution of energy in quasi-static MHD turbulence, starting from isotropic initial turbulence, is the result of an essentially angular transfer, as we have shown above with DNS and the EDQNM model, and as was observed in towed-grid turbulence in mercury by Alemany *et al.* (1979); Caperan & Alemany (1985). These authors, using interaction parameters between $N \simeq 0.6$ and 1.17, also observe the appearance of a k_{\parallel}^{-3} scaling for the axial kinetic energy spectrum $E_{\parallel}(k_{\parallel})$, that progressively replaces the Kolmogorov scaling $k_{\parallel}^{-5/3}$ over an increasingly wider wavenumber range. The complete $E_{\parallel}(k_{\perp}, k_{\parallel})$ distribution, plotted on figure 12, pictures the spectral equilibrium

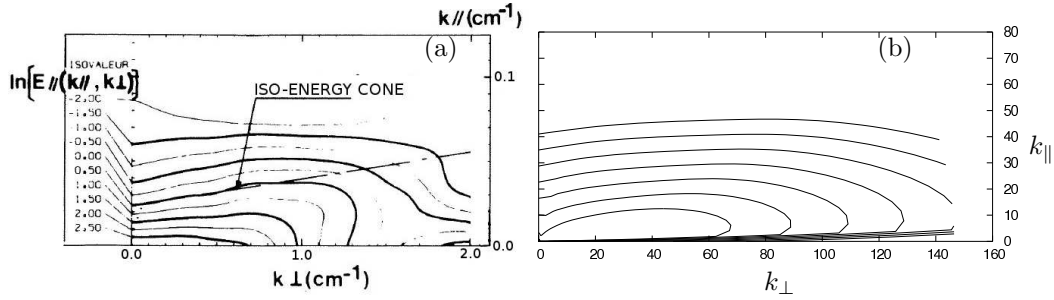


Figure 12: Iso-contours of the two-dimensional spectral distribution of the axial kinetic energy $E_{\parallel}(k_{\perp}, k_{\parallel})$ in logarithm scale. (a) Figure extracted from Caperan & Alemany (1985), at $Re \simeq 1800$ and the interaction parameter $N \simeq 0.6$. The conical spectral distribution is shown. (b) EDQNM2 result at $t^* = 12$, $Re = 333$ and $N = 5$, with iso-contour levels from -60 to -20 by steps of 5.

of energy, due to both Joule dissipation—that drains energy towards the transverse 2D plane—and nonlinear inertial transfers. As argued by Caperan & Alemany (1985), the equilibrium between the two phenomena should lead to a conical distribution of spectral energy, which seems to be observed on figure 12(a). The same quantity computed with EDQNM is plotted on figure 12(b). The model permits this refined representation since it provides a smooth distribution of the spectra, hardly available in DNS. The comparison between the two panels of figure 12 suggests strong similarities in the dynamical equilibrium obtained in the experiment and in the EDQNM model. [From figure 10 which presents angular spectra, but contains the same information as shown differently on figure 12(b), we believe that an equivalent agreement would be obtained with DNS.] One must bear in mind, however, that the dimensional scalings of both plots of figure 12 are different, so that no quantitative agreement is claimed.

In order to investigate further inertial transfers in the QS MHD turbulent flow, we compute energy transfer spectra. They are presented on figure 13 at the same time $t^* = 5$ as the spectra of figure 10. In DNS, the spherically averaged transfer spectrum is directly computed from the nonlinear term $\mathbf{s} = \mathbf{u} \times \boldsymbol{\omega}$, with $\boldsymbol{\omega} = \nabla \times \mathbf{u}$, as

$$T_i(k) = \sum_{k-\Delta k \leq |\mathbf{k}| < k+\Delta k} \frac{1}{2} [\hat{u}_i(\mathbf{k})\hat{t}_i(-\mathbf{k}) + \hat{u}_i(-\mathbf{k})\hat{t}_i(\mathbf{k})] \quad (26)$$

where $\hat{\mathbf{t}} = -k^2[\mathbf{k} \times (\mathbf{k} \times \hat{\mathbf{s}})]$. We focus here on equatorial modes $\mathbf{k} \perp \mathbf{B}_0$ and we distinguish the axial equatorial transfer $T_a(k_{\perp})$ and the transverse equatorial transfer $T_t(k_{\perp})$. In EDQNM closures, these quantities are directly obtained as

$$T_t(k_{\perp}) = T^{(e)}(k, \theta = \pi/2) - T^{(Z)}(k, \theta = \pi/2) \quad (27)$$

$$T_a(k_{\perp}) = T^{(e)}(k, \theta = \pi/2) + T^{(Z)}(k, \theta = \pi/2) . \quad (28)$$

We observe an overall good agreement between DNS and EDQNM on figure 13. For $N = 1$, one observes a reduced transverse transfer compared to the axial one, both in DNS and in EDQNM closures. For $N = 5$, DNS and EDQNM2 clearly display a positive transfer at large scales, characteristic of an inverse cascade of kinetic energy. As described in Favier *et al.* (2010), the transverse component of the velocity behaves as in two-dimensional turbulence, with the axial velocity component acting as a passive scalar, thus characterised by a classical direct cascade. This inverse cascade of transverse velocity explains the reduction of dissipation and thus the dominance of transverse kinetic energy at large times (see figure 6). Note that EDQNM1 is unable to reproduce the inverse cascade observed in DNS and EDQNM2. Finally, the oscillations observed in the DNS transfers for $N = 5$ could be explained by the fact that DNS yields one particular realization of the flow. The statistics of a flow can differ significantly from what is computed from an instantaneous flow field, in particular in the large scales. We therefore do not exclude that the double positive lobe of $T_t(k_{\perp})$ vanishes if we average over more flow realizations.

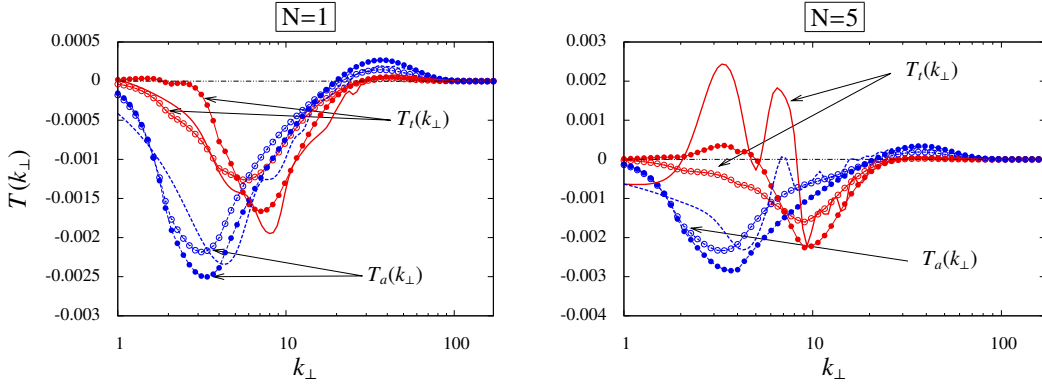


Figure 13: Equatorial kinetic energy transfer spectra at dimensionless times $t^* = 5$. — DNS, \circ EDQNM1 and \bullet EDQNM2.

7 Additional results accessible only with the EDQNM closure model

We have presented in section 6 a comparison of the EDQNM2 closure model with DNS, which validates the results of the model for the given range of parameters attainable with DNS. However, due to the very way it is constructed and implemented, the added value of the EDQNM model is clearly to allow the investigation of an extended range of turbulent regimes. In the following two sections, we investigate high Reynolds number turbulence, currently out of the grasp of Direct Numerical Simulations (section 7.1), and a derived model for the limit case of two-dimensional three-components turbulence (section 7.2).

7.1 High Reynolds number turbulence

In this section, we address an important question of this article: are DNS predictions reliable to understand high Reynolds number quasi-static MHD turbulence given the moderate hydrodynamic Reynolds number? We use the EDQNM model at higher Reynolds number to answer this question. The number of wave numbers considered in EDQNM models has to be increased, along with the angular discretization and triadic interactions count. The following simulations are based on 100 wave numbers, 48 polar angles and 48 angles for the direction of the plane of the triad around \mathbf{k} (denoted λ in appendix A). The initial Reynolds number is increased from the previous value of $Re \approx 333$ up to $Re \approx 2 \times 10^5$. The initial condition for these high Reynolds simulations is similar to the one used for previous EDQNM simulations, except that the inertial range of the initial energy spectra is extended to higher wave numbers.

Equatorial spectra are gathered on figure 14. First, the lowermost spectra on the figure recall the previous 512^3 DNS results (these spectra are shifted down by six decades). The corresponding cross-over wave number is $k_{\perp}^c \simeq 171$. The intermediate results correspond to EDQNM2, obtained with an initial Reynolds $Re \simeq 2200$. The DNS resolution required to accurately simulate such a flow is about 1500^3 Fourier modes. The results are qualitatively unchanged, but the slopes k_{\perp}^{-1} and k_{\perp}^{-3} appear more clearly, even more so for the top curves on the figure, corresponding to an initial Reynolds number $Re \simeq 2 \times 10^5$. The corresponding DNS resolution using pseudo-spectral methods would be about 6000^3 Fourier modes. We note also that the cross-over wave number k_{\perp}^c defined by $\Phi^1(k_{\perp}^c) \approx \Phi^2(k_{\perp}^c)$ increases with the value of the Reynolds number, to $k_{\perp}^c \simeq 35$ for $Re \simeq 2200$, and $k_{\perp}^c \simeq 50$ for $Re \simeq 2 \times 10^5$.

7.2 A model for 2D-3C turbulence

In two-dimensional three-components (2D-3C) flows, the velocity field contains three non zero components, which only vary in two directions (the transverse plane, say), and are independent of

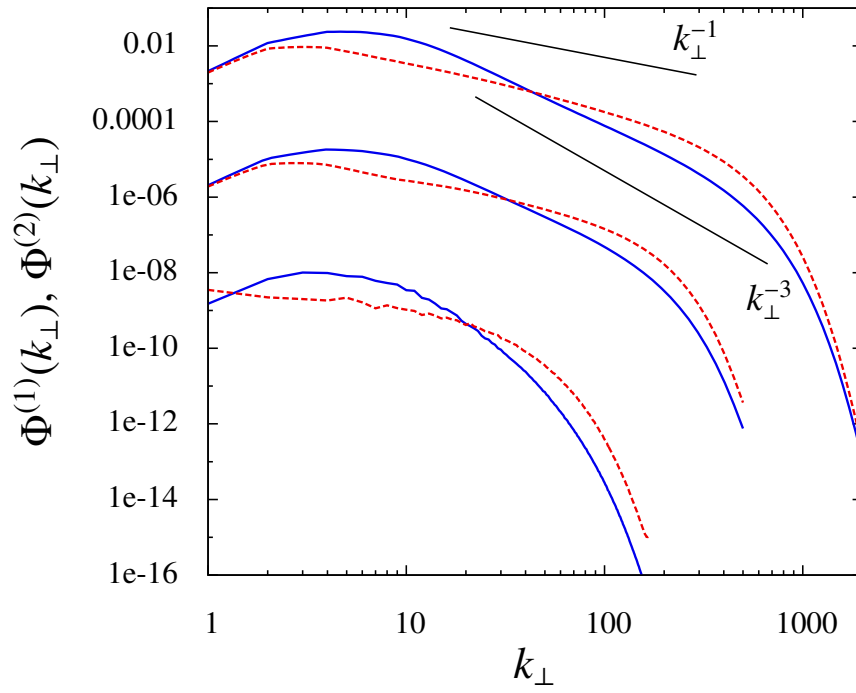


Figure 14: Poloidal/Toroidal decomposition of the equatorial energy spectra. The interaction parameter is $N = 5$. All the results are plotted at $t^* \approx 5$. From bottom to top: DNS using 512^3 Fourier modes (shifted down by 6 decades), EDQNM2 corresponding to a spectral resolution of 1500^3 Fourier modes (shifted down by 3 decades) and EDQNM2 corresponding to a spectral resolution of 6000^3 Fourier modes.

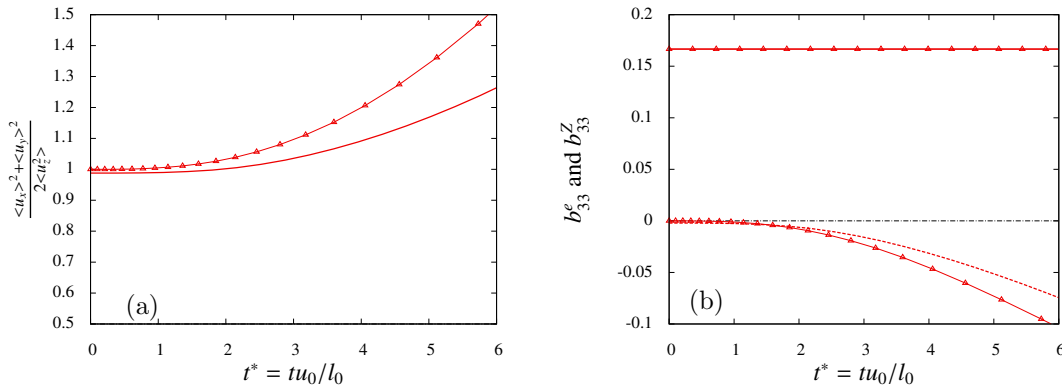


Figure 15: (a) Ratio between horizontal and vertical kinetic energy for 2D-3C turbulence. (b) Anisotropic tensor b_{33} and its decomposition. — DNS and \triangle EDQNM.

the third direction (axial). The analogy between 2D-3C turbulence and the final state of quasi-static MHD turbulence is supported by theoretical (Montgomery & Turner (1982)) and numerical (Favier *et al.* (2010)) evidences. In previous sections, we found some indications, using EDQNM spectral closures, that this statement, supported by DNS at moderate Reynolds number, is valid for higher values of the Reynolds number, using EDQNM spectral closures. This last section is devoted to the comparison between DNS and EDQNM closures in a 2D-3C context.

Theoretically, to consider 2D-3C turbulence is equivalent to considering purely 2D turbulence with a passive scalar (the latter being the vertical component of the velocity). As shown by Cambon & Godeferd (1993) (see appendix A.2), the EDQNM1 model for anisotropic turbulence reduces exactly to a 2D-3C model for Φ^1 and Φ^2 , in which Φ^2 plays the same role as the scalar spectrum in 2D EDQNM (Lesieur & Herring (1985)).

The previous 3D simulations tend to a 2D-3C state but this transition is triggered by dissipative effects so that the remaining energy is very small. To numerically investigate the 2D-3C state at high Reynolds numbers, we consider initially 2D-3C turbulence using both a 2D pseudo-spectral code and a 2D version of EDQNM closures presented above which include a passive scalar (considered here as the axial velocity component). We use 1024^2 Fourier modes for the DNS and 51 wave numbers for the spectral discretization of EDQNM. The initial condition is the same in both cases: $\Phi^1(k, t^* = 0) = \Phi^2(k, t^* = 0) = 10^{-4}k^2 \exp(-(k/k_m)^2)$, and $k_m = 8$. The molecular viscosity is fixed to $\nu = 5 \times 10^{-5}$ which corresponds to an initial Reynolds number of about 10^3 . In the 3D axisymmetric case, the equatorial initial condition was also characterised by $\Phi^1(k_\perp) = \Phi^2(k_\perp)$, the main difference being that triple correlations were initially non zero. Here, the initial condition is a random Gaussian velocity field with an integral scale $l_0 \approx 0.32$ and *rms* velocity $u_0 \approx 0.18$, hence with zero third-order moments.

The ratio between transverse and axial kinetic energies is presented in figure 15(a). As expected, the initial value is about unity. As time increases, the inverse cascade of the horizontal velocity field develops so that the dissipation of horizontal components is reduced. This phenomenon is responsible for the growth of $\langle u_x^2 + u_y^2 \rangle / \langle u_z^2 \rangle$. In the 3D axisymmetric case, one first observes a decrease of this quantity (see figure 6(a)). This is due to the transition from a 3D initial state to a quasi-two-dimensional state in which the inverse cascade occurs. Figure 15(a) also shows that the EDQNM evolution is faster (maybe from the fact that, in the EDQNM model, triple correlations—energy transfers— build up instantly).

On figure 15(b), the anisotropic tensor b_{33} and its $b_{33}^{(e)}$, $b_{33}^{(z)}$ decomposition are presented. Since the flow is 2D-3C, all axial derivatives are zero, so that all the energy is concentrated in the transverse plane. In that case, b_{33}^e reaches its maximum value $1/6$ (see Cambon *et al.* (1997)). The polarization is initially very small, and becomes negative at larger times due to the dominance of toroidal (also transverse) energy with respect to the poloidal (also axial) energy.

Finally, the poloidal/toroidal decomposition of the equatorial energy spectra is plotted in figure 16. EDQNM and DNS are in very good agreement (again with the minor exception of the dissipative range). This result confirms the previous k_\perp^{-3} and k_\perp^{-1} scalings for the axial and transverse

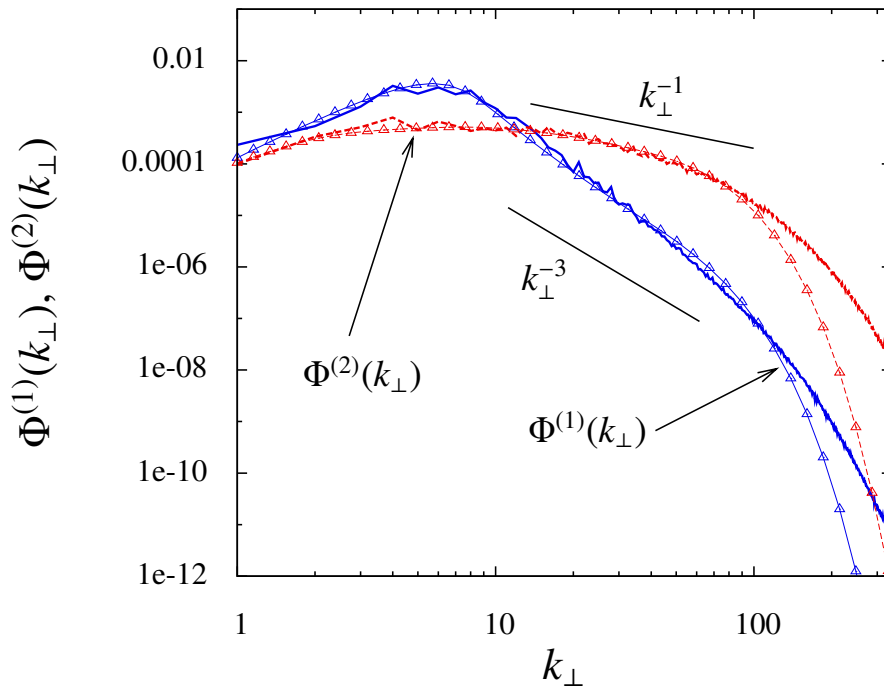


Figure 16: Poloidal/Toroidal decomposition of the equatorial energy spectra for two and a half dimensional turbulence. All the results are plotted at $t^* \approx 5$. — DNS, \triangle EDQNM.

velocity components, similar to those observed on figure 11 for the three-dimensional simulations. The asymptotic state of quasi-static MHD turbulence is therefore very similar to two-dimensional turbulence advecting a passive scalar.

8 Conclusion and final remarks

In this paper, we have investigated the dynamics and the detailed anisotropy of magneto-hydrodynamic turbulence in the quasi-static approximation at small magnetic Reynolds number, using Direct Numerical Simulations and a two-point statistical closure of EDQNM type. By essence, such closures consider statistical averages, which is a key advantage when considering turbulent flows, for two reasons: first, only one simulation is required to obtain averaged results, in contrast with the large number of realizations needed in DNS (typically more than a dozen); secondly, the obtained averages are smoother functions than in DNS, all the more if one considers high order moments (*e.g.* third-order correlations). In terms of computational cost, isotropic EDQNM or the 2D-3C model presented in section 7.2 are thousands of times less costly than equivalent DNS. The axisymmetric anisotropic EDQNM2 model abandons one symmetry with respect to the isotropic context, thus the convolution integral is an order of magnitude more expensive. Therefore EDQNM2 computations, although not as cpu and memory demanding as DNS by a factor of about 10 in the present parameter range, are also run on a parallel computer. The extension of two-point statistical closures to bounded turbulent flows (Kraichnan (1972); Turner (2000); Laporta (1995)), however, is analytically and computationally challenging.

In terms of statistical analysis, the closure allows for easy access to the general decomposition of tensors in the axisymmetric flow, such that refined statistics of turbulence can be used for characterizing anisotropy. The poloidal/toroidal decomposition of the velocity field and related second-order statistics permits the computation of a polarization tensor, which is a key indicator of whether the anisotropic mechanism is of linear nature—the Joule dissipation—or due to more complex nonlinear interactions. (The extraction of equivalent second-order statistics in physical space, although formally possible, would be hardly tractable, because of the differential operators involved). There remains the possibility to obtain such statistics by post-processing DNS data

fields, although with all the inaccuracies and sub-sampling issues due to limited resolutions. Clearly, DNS discretization is insufficient in the very large scale range of the spectrum, and EDQNM is better off in this range and very adequate in the inertial range; less so in the smallest scales.

We have nonetheless compared results of the EDQNM closure model with those of 512^3 DNS. The EDQNM1 version of the model and the EDQNM2 one provide slightly different results, but the overall agreement with DNS is quite good. Comparisons involve kinetic energy and enstrophy, kinetic energy spectra and directional velocity correlation lengths. The latter allow us to address the question of numerical confinement due to the finiteness of the computational box in DNS, of importance in QS MHD turbulence in which the axial velocity correlation length increases tremendously.

Several quantities were used to assess the level of anisotropy in the flow. Starting with initial conditions of isotropic turbulence, the ratios of transverse energy (resp. enstrophy) to axial energy (resp. enstrophy), the Shebalin angles and the off-diagonal components of the Reynolds stress tensor indicate all that the flow dynamics becomes closer to a two-dimensional three-components state. However, upon investigation of transverse and axial energy spectra, we are able to define a cross-over wavenumber below which the toroidal contribution dominates over the poloidal one, with a reversal of this order in the larger wave numbers or small scales. Not only are these predictions of DNS confirmed in a satisfactory quantitative manner by EDQNM, but the model allows to reach higher Reynolds numbers than permitted by DNS. The dynamics is not significantly altered at higher Reynolds numbers reached with the closure model. However, asymptotic scaling behaviour appears only very slowly. If a qualitative understanding of QS MHD is called for, both DNS and closure models are applicable. However, if scaling ranges and inertial range behaviour are of interest, two-point closures remain an indispensable tool.

We conclude by noting that rotating turbulence bears strong similarities with QS MHD turbulence. In both cases, a transition from 3D to 2D structure is observed, and the 2D-2C trend is evidenced by the separation of $L_{11}^{(3)}$ and $L_{33}^{(3)}$ integral scales, due to the growth of polarization in the horizontal transverse wave plane. This transition originates from the *linear* Joule dissipation term in QS MHD, but from *nonlinear* interactions dominated by cubic transfer terms such as $T^{(e)}$, when solid body rotation acts. Therefore, QS MHD turbulence may eventually become fully two-dimensional, whereas complete two-dimensionalization cannot be achieved in rotating turbulence in absence of additional phenomena.

The authors thank the computing centre IDRIS of CNRS for the allocation of CPU time under project numbers 071433 and 022206. We also would like to thank the referees for their suggestions leading to improvements of the paper.

A Detail on anisotropic EDQNM equations and their numerical calculation

A.1 EDQNM closure for the spectral energy transfers

In section 3, the important term to specify is the quasi-normal one denoted $\Omega_{ss's''}^{(QN)}(\mathbf{k}, \mathbf{p}, t')$, for modelling the fourth-order terms in (12) which is exactly given as a sum of quadratic terms from the set

$$e = e(\mathbf{k}, t'), e' = e(\mathbf{p}, t'), e'' = e(\mathbf{q}, t'), Z = Z(\mathbf{k}, t') \quad (29)$$

in the case of a zero helicity flow. (The helicity, in contrast with the polarization anisotropy, remains zero if initially zero.) Instead of expressing $\Omega_{ss's''}^{(QN)}$, it is simpler to derive its contribution to $T^{(e)}$ and $T^{(Z)}$, as was done for the EDQNM model for rotating turbulence, so that the numerical code for the EDQNM models used here is easily derived from the one for rotating turbulence (see *e.g.* Bellet *et al.* (2006)).

Detailed equations for $T^{(e)}$ and $T^{(Z)}$ in the EDQNM2 model are

$$T^{(e)} = \frac{1}{2^3} \sum_{ss's''} \int \frac{2p}{k} \frac{C_{kpq}^2}{\theta_{kpq}^{-1} + M_0^2 (\cos^2 \theta_k + \cos^2 \theta_p + \cos^2 \theta_q)}$$

$$\begin{aligned}
& \left[A_1(sk, s'p, s''q)e''(e - e') + A_2(sk, s'p, s''q)e^{2is''\lambda''} eZ(s''\mathbf{q}) + A_3(sk, s'p, s''q)e^{2is\lambda} e''Z(s\mathbf{k}) \right. \\
& \quad \left. - A_5(sk, s'p, s''q)e^{2is''\lambda''} e'Z(s''\mathbf{q}) \right. \\
& \quad \left. + A_4(sk, s'p, s''q) \left(e^{2is''\lambda''+2is\lambda} Z(s''\mathbf{q})Z(s\mathbf{k}) - e^{2is''\lambda''+2is'\lambda'} Z(s''\mathbf{q})Z(s'\mathbf{p}) \right) \right] d^3\mathbf{p} \quad (30)
\end{aligned}$$

and

$$\begin{aligned}
T^{(z)} &= \frac{1}{2^3} \sum_{s's''} \int \frac{2p}{k} \frac{C_{kpq}^2 e^{-2i\lambda}}{\theta_{kpq}^{-1} + M_0^2(\cos^2\theta_k + \cos^2\theta_p + \cos^2\theta_q)} \\
& \left[A_3(k, -s'p, -s''q)e''(e' - e) + A_4(k, -s'p, -s''q)e^{2is''\lambda''} eZ(s''\mathbf{q}) + A_1(k, -s'p, -s''q)e^{2i\lambda} e''Z(s\mathbf{k}) \right. \\
& \quad \left. - A_5(k, -s'p, -s''q)e^{2is'\lambda'} e''Z(s'\mathbf{p}) \right. \\
& \quad \left. + A_2(k, -s'p, -s''q) \left(e^{2is''\lambda''+2i\lambda} Z(s''\mathbf{q})Z(s\mathbf{k}) - e^{2is''\lambda''+2is'\lambda'} Z(s''\mathbf{q})Z(s'\mathbf{p}) \right) \right] d^3\mathbf{p} \quad (31)
\end{aligned}$$

The geometric factors A_1 to A_5 are given in the appendix of Cambon *et al.* (1997), and in Sagaut & Cambon (2008); they depend only on the moduli k, p, q , ‘signed’ by the polarization signs of helical modes, $s = \pm 1, s' = \pm 1, s'' = \pm 1$. C_{kpq} depends only on the geometry of the triad as well, such that

$$\frac{\sin(\widehat{\mathbf{p}, \mathbf{q}})}{k} = \frac{\sin(\widehat{\mathbf{q}, \mathbf{k}})}{p} = \frac{\sin(\widehat{\mathbf{k}, \mathbf{p}})}{q} = C_{kpq}. \quad (32)$$

The internal triadic angles λ, λ' and λ'' denote the angle of rotation of the plane of the triad around $\mathbf{k}, \mathbf{p}, \mathbf{q}$, respectively. Integration variables, which generate all the other terms at fixed \mathbf{k} , are p, q , as in isotropic EDQNM, and λ , relevant in the axisymmetric case, and discretized as well.

The only semi-empirical term in the formulae above is the viscous plus eddy damping term denoted θ_{kpq}^{-1} since it is homogeneous to an inverse time scale, with

$$\theta_{kpq}^{-1} = \nu(k^2 + p^2 + q^2) + \vartheta(k, t) + \vartheta(p, t) + \vartheta(q, t), \quad (33)$$

in which $\vartheta(k, t) = A \left(\int_0^k p^2 E(p, t) dp \right)^{1/2}$ may be viewed as a straining decorrelation time scale of small turbulent structures by larger ones. Here, $E(k)$ is the classical energy spectrum and $A = 0.355$ is the only adjusted constant of the model, computed from the Kolmogorov constant C_K with the relation $C_K \simeq 2.76A^{2/3}$ (Lesieur & Ossia (2000)).

The EDQNM1 version of the closure model does not incorporate linear Joule dissipation terms proportional to M_0^2 in equations (30) and (31). It is therefore generic to any turbulent case, in which the distortion only appears explicitly in a linear term added to the dissipation one.

A.2 Recovering the 2D-3C case

This was done by Cambon & Godefert (1993) as follows. In the 2D-3C limit, e and Z are concentrated in the plane k_{\parallel} (or k_3 here) = 0, so that

$$e(\mathbf{k}, t) = e^{(2D)}(k, t)\delta(k_{\parallel}), Z(\mathbf{k}, t) = Z^{(2D)}(k, t)\delta(k_{\parallel}), \quad (34)$$

and similarly for $T^{(e, Z)}$. The Jacobian from (p_1, p_2) to (p, q) variables is now $1/\sqrt{1-x^2}$, only planar triads ($k_{\parallel} = p_{\parallel} = q_{\parallel} = 0$) are called into play, and $e^{2i\lambda} = e^{2i\lambda'} = e^{2i\lambda''} = -1$. Accordingly, the 2D counterparts of Lin equation for Φ^1 and Φ^2 are derived as

$$\left(\frac{\partial}{\partial t} + 2\nu k^2 \right) \Phi^1(k, t) = T^1(k, t) = T^{(e), 2D}(k, t) - T^{(Z), 2D}(k, t) \quad (35)$$

and

$$\left(\frac{\partial}{\partial t} + 2\nu k^2 \right) \Phi^2(k, t) = T^2(k, t) = T^{(e), 2D}(k, t) + T^{(Z), 2D}(k, t), \quad (36)$$

with

$$T^1(k, t) = \int \int_{\Delta_k} \frac{2kp\theta_{kpq}}{\sqrt{1-x^2}} (xy + 2z^3 - z) \Phi^1(q, t) (\Phi^1(p, t) - \Phi^1(k, t)) dpdq \quad (37)$$

and

$$T^2(k, t) = \int \int_{\Delta_k} \frac{2kp\theta_{kpq}}{\sqrt{1-x^2}} (xy + z) \Phi^1(q, t) (\Phi^2(p, t) - \Phi^2(k, t)) dpdq. \quad (38)$$

It is shown that the 2D contribution from toroidal (horizontal in 2D) velocity is governed by the classical isotropic EDQNM equation restricted to 2D (Leith 1971, Pouquet *et al.* 1975), whereas the 2D contribution from poloidal (vertical in this limit) velocity is governed by the isotropic EDQNM equation in 2D for a passive scalar.

More conventional relationship is found in term of the averaged spectrum using $e^{(2D)}(k, t) = E(k, t)/(2\pi k)$, as for the 3D isotropic case, in which $e(k, t) = E(k, t)/(4\pi k^2)$.

B RDT solutions for the correlation lengths

The linear inviscid evolution of the spectral tensor is immediately found as

$$e(k, \mu, t) = \frac{E(k, 0)}{4\pi k^2} \exp(-2M_0^2 \mu^2 t), \quad Z(k, \mu, t) = 0, \quad (39)$$

with $\mu = \cos \theta$ and θ the angle between \mathbf{k} and the vertical.

Two-dimensional energy components are invariant when defined as

$$\langle u_3^2 \rangle(t) L_{33}^{(3)}(t) = \frac{1}{3} \mathcal{K}_0 l_0, \quad \langle u_1^2 \rangle(t) L_{11}^{(3)}(t) = \langle u_2^2 \rangle(t) L_{22}^{(3)}(t) = \frac{1}{6} \mathcal{K}_0 l_0, \quad (40)$$

because they involve only contributions of e and Z at $\mu = 0$. \mathcal{K}_0 and l_0 are the initial kinetic energy and initial integral scale respectively. Kinetic energy and individual Reynolds stress components are given by

$$\mathcal{K}(t) = \mathcal{K}_0 \int_0^1 \exp(-2M_0^2 \mu^2 t) d\mu, \quad (41)$$

and

$$\langle u_3^2 \rangle(t) = \frac{\mathcal{K}_0}{2} \int_0^1 (1 - \mu^2) \exp(-2M_0^2 t \mu^2) d\mu, \quad \langle u_1^2 \rangle(t) = \frac{\mathcal{K}_0}{4} \int_0^1 (1 + \mu^2) \exp(-2M_0^2 t \mu^2) d\mu, \quad (42)$$

in agreement with $d^3 \mathbf{k} = 2\pi k^2 dk d\mu$ using polar-spherical coordinates for \mathbf{k} and axisymmetry.

The inviscid RDT time development of all relevant statistical quantities is derived analytically, in terms of the error function erf (exact relationship available from the authors upon request). The dominant terms in the evolution yield the following simple scalings: the kinetic energy decays as $M_0^{-1} \Gamma(\infty) (2t)^{-1/2}$, as well as the Reynolds stress components; integral length scales with axial separation behave as $M_0 l_0 \sqrt{t}$. Upon introduction of viscosity through the integrating factor $e^{-2\nu k^2 t}$ in the integrands of equations (41) and (42), the viscous RDT solution is recovered, this time depending on the explicit shape of the spectrum $E(k)$. For example, the RDT evolution of integral lengthscales may be compared to the evolution plotted on figure 2, and exhibit a linear evolution instead as the above inviscid \sqrt{t} behaviour.

References

- ALEMANY, A., MOREAU, R., SULEM, P. L & FRISCH, U. 1979 Influence of an external magnetic field on homogeneous MHD turbulence. *J. Mécan.* **18**, 277–313.
- BATCHELOR, G.K. 1959 Small-scale variation of convected quantities like temperature in turbulent fluid. *J. Fluid Mech.* **5**, 113.
- BELLET, F., GODEFERD, F.S., SCOTT, J.F. & CAMBON, C. 2006 Wave-turbulence in rapidly rotating flows. *J. Fluid Mech.* **562**, 83–121.

- BOS, W.J.T., KADOCH, B., SCHNEIDER, K. & BERTOGLIO, J.-P. 2009 Inertial range scaling of the scalar flux spectrum in two-dimensional turbulence. *Physics of Fluids* **21** (11), 115105.
- BURATTINI, P., KINET, M., CARATI, D. & KNAEPEN, B. 2008a Anisotropy of velocity spectra in quasistatic magnetohydrodynamic turbulence. *Phys. Fluids* **20** (065110).
- BURATTINI, P., KINET, M., CARATI, D. & KNAEPEN, B. 2008b Spectral energetics of quasi-static MHD turbulence. *Physica D* **237**, 2062–2066.
- CAMBON, C. 1990 Homogeneous MHD turbulence at weak magnetic Reynolds numbers: approach to angular-dependent spectra. In *Advances in Turbulence Studies* (ed. H. Branover & Y. Unger), *Progress in Astronautics and Aeronautics*, vol. 149, pp. 131–145. AIAA, Washington DC.
- CAMBON, C. & GODEFERD, F. S. 1993 Inertial transfers in freely decaying rotating, stably-stratified, and MHD turbulence. In *Progress in Turbulence Research* (ed. H. Branover & Y. Unger), *Progress in Astronautics and Aeronautics*, vol. 162, pp. 150–168. AIAA, Washington DC.
- CAMBON, C. & JACQUIN, L. 1989 Spectral approach to non-isotropic turbulence subjected to rotation. *J. Fluid Mech.* **202**, 295–317.
- CAMBON, C., MANSOUR, N. N. & GODEFERD, F. S. 1997 Energy transfer in rotating turbulence. *J. Fluid Mech.* **337**, 303–332.
- CAPERAN, PH. & ALEMANY, A. 1985 Turbulence homogène MHD à faible nombre de Reynolds magnétique. étude de la transition vers la phase quasi bidimensionnelle et caractérisation de son anisotropie. *J. Méca. Théor. Appl.* **4** (2), 175–200.
- FAVIER, B., GODEFERD, F.S., CAMBON, C. & DELACHE, A. 2010 On the two-dimensionalization of quasi-static MHD turbulence. *Phys. Fluids* **22**, 075104.
- GODEFERD, F. S. & STAQUET, C. 2003 Statistical modelling and direct numerical simulations of decaying stably-stratified turbulence: Part 2: Large scales and small scales anisotropy. *J. Fluid Mech.* **486**, 115–150.
- HERRING, J.R. 1974 Approach of axisymmetric turbulence to isotropy. *Phys. Fluids* **17**, 859–872.
- ISHIDA, T. & KANEDA, Y. 2007 Small-scale anisotropy in magnetohydrodynamic turbulence under a strong uniform magnetic field. *Phys. Fluids* **19** (075104), 10 pages.
- JACQUIN, L., LEUCHTER, O., CAMBON, C. & MATHIEU, J. 1990 Homogeneous turbulence in the presence of rotation. *J. Fluid Mech.* **125**, 505–534.
- VON KÁRMÁN, T. & LIN, C. C. 1949 On the concept of similitude in the theory of isotropic turbulence. *Rev. Modern Phys.* **21** (3), 516–519.
- KNAEPEN, B., KASSINOS, S. & CARATI, D. 2004 Magnetohydrodynamic turbulence at moderate Reynolds number. *J. Fluid Mech.* **513**, 199–220.
- KNAEPEN, B. & MOREAU, R. 2008 Magnetohydrodynamic turbulence at low magnetic Reynolds number. *Annu. Rev. Fluid Mech.* **40**, 25–45.
- KRAICHNAN, R.H. 1972 Test-field model for inhomogeneous turbulence. *J. Fluid Mech.* **56**, 287–304.
- LAPORTA, A. 1995 Spectral study and modelisation of an inhomogeneous turbulence. PhD thesis, cole Centrale de Lyon, in french.
- LESIEUR, M. & HERRING, J. 1985 Diffusion of a passive scalar in two-dimensional turbulence. *J. Fluid Mech.* **161**, 77–95.
- LESIEUR, M. & OSSIA, S. 2000 3d isotropic turbulence at very high Reynolds numbers: Eddy study. *J. of Turb.* **1** (Art. No 7), 25 pages.

- MATSUMOTO, T. 2009 Anomalous scaling of three-dimensional rayleigh-taylor turbulence. *Phys. Rev. E* **79**, 055301.
- MOFFATT, H.K. 1967 On the suppression of turbulence by a uniform magnetic field. *J. Fluid Mech.* **28**, 571–592.
- MONTGOMERY, D. & TURNER, L. 1982 Two-and-a-half-dimensional magnetohydrodynamic turbulence. *Phys. Fluids* **25(2)**, 345–349.
- OKAMOTO, N., DAVIDSON, P. A. & KANEDA, Y. 2010 On the decay of Low-Magnetic-Reynolds-Number turbulence in an imposed magnetic field. *J. Fluid Mech.* **651**, 295–318.
- SCHUMANN, U. 1976 Numerical simulation of the transition from three- to two-dimensional turbulence under a uniform magnetic field. *J. Fluid Mech.* **74**, 31–58.
- SHEBALIN, J.V., MATTHAEUS, W.H. & MONTGOMERY, D. 1983 Anisotropy in MHD turbulence due to a mean magnetic field. *J. Plasma Phys.* **29**, 525.
- STAPLEHURST, P. J., DAVIDSON, P. A. & DALZIEL, S. B. 2008 Structure formation in homogeneous freely decaying rotating turbulence. *J. Fluid Mech.* **598**, 81–105.
- TURNER, L. 2000 Using helicity to characterize homogeneous and inhomogeneous turbulent dynamics. *J. of Fluid Mech.* **408**, 205–238.
- VOROBEV, A., ZIKANOV, O., DAVIDSON, P.A. & KNAEPEN, B. 2005 Anisotropy of MHD turbulence at low magnetic Reynolds number. *Phys. Fluids* **17**, 125105.
- WALEFFE, F. 1992 The nature of triad interactions in homogeneous turbulence. *Phys. Fluids* **A-4**, 350–363.
- WALEFFE, F. 1993 Inertial transfers in the helical decomposition. *Phys. Fluids* **A-5**, 677–685.
- ZHOU, Y. 2010 Renormalization group theory for fluid and plasma turbulence. *Phys. Rep.* **488**, 1–49.
- ZHOU, Y. & MATTHAEUS, W.H. 2005 Phenomenology treatment of magnetohydrodynamic turbulence with nonequipartition and anisotropy. *Phys. Plasmas* **12**, 056503.
- ZHOU, Y., MATTHAEUS, W.H. & DMITRUK, P. 2004 Magnetohydrodynamic turbulence and time scales in astrophysical and space plasmas. *Rev. Mod. Phys.* **76**, 1015–1035.